TRPM8 inhibits endothelial cell migration via a non-channel function by trapping the small GTPase Rap1

Tullio Genova,[1,3]* Guillaume P. Grolez,[4]* Chiara Camillo,[6] Michela Bernardini,[1,4] Alexandre Bokhobza,[4] Elodie Richard,[5] Marco Scianna,[7] Loic Lemonnier,[4] Donatella Valdembri,[6] Luca Munaron,[1,2] Mark R. Philips,[8] Virginie Mattot,[9] Guido Serini,[6] Natalia Prevarskaya,[4]** Dimitra Gkika,[4]** and Alessandra Fiorio Pla[1,2,4]**

[1]Department of Life Sciences and Systems Biology, [2]Nanostructured Interfaces and Surfaces Centre of Excellence, and [3]Department of Surgical Sciences, C.I.R. Dental School, University of Torino, Torino, Italy
[4]Laboratoire de Physiologie cellulaire, Institut National de la Santé et de la Recherche Médicale U1003, Laboratory of Excellence, Ion Channels Science and Therapeutics and [5]BICeL Campus Lille1, FR3688 FRABio, Université de Lille, Villeneuve d'Ascq, France
[6]Laboratory of Cell Adhesion Dynamics, Candiolo Cancer Institute, Fondazione del Piemonte per l'Oncologia, Istituto di Ricovero e Cura a Carattere Scientifico, Department of Oncology, University of Torino School of Medicine, Candiolo, Italy
[7]Department of Mathematical Sciences, Politecnico di Torino, Torino, Italy
[8]Cancer Institute of Biomolecular Medicine, New York University School of Medicine, New York, NY
[9]Centre National de la Recherche Scientifique, Institut Pasteur de Lille, UMR 8161 – Mechanisms of Tumorigenesis and Target Therapies, Universite de Lille, Lille, France

Endothelial cell adhesion and migration are critical steps of the angiogenic process, whose dysfunction is associated with tumor growth and metastasis. The TRPM8 channel has recently been proposed to play a protective role in prostate cancer by impairing cell motility. However, the mechanisms by which it could influence vascular behavior are unknown. Here, we reveal a novel non-channel function for TRPM8 that unexpectedly acts as a Rap1 GTPase inhibitor, thereby inhibiting endothelial cell motility, independently of pore function. TRPM8 retains Rap1 intracellularly through direct protein–protein interaction, thus preventing its cytoplasm–plasma membrane trafficking. In turn, this mechanism impairs the activation of a major inside-out signaling pathway that triggers the conformational activation of integrin and, consequently, cell adhesion, migration, in vitro endothelial tube formation, and spheroid sprouting. Our results bring to light a novel, pore-independent molecular mechanism by which endogenous TRPM8 expression inhibits Rap1 GTPase and thus plays a critical role in the behavior of vascular endothelial cells by inhibiting migration.

Introduction

Tissue vascularization and angiogenesis represent essential processes by which organs obtain appropriate blood supply and nutrients under physiological conditions. In contrast, many diseases are associated with dysfunctions of these processes. In particular cancer growth and metastasis are strictly dependent on tumor vascularization, which is promoted by the tumor cells themselves through the secretion of several growth factors.

Endothelial cell (EC) adhesion and migration are critical steps of the angiogenic process, in which activated ECs, led by tip cells, migrate toward a chemoattractant angiogenic signal consisting of growth factors that are secreted by tumor cells and their stroma and give rise to an integrated vascular network (Potente et al., 2011). In this process, EC adhesion to provisional ECM proteins such as fibronectin (FN) is mediated by α5β1- and αv-containing integrin receptors, which cooperate in remodeling the vasculature during angiogenesis (Serini et al., 2006; van der Flier et al., 2010). Small G proteins belonging to the Ras-associated protein (Rap) branch of the wider Ras superfamily have been implicated in a variety of integrin-mediated "inside-out" signaling events (Reedquist et al., 2000; Lafuente et al., 2004; Chrzanowska-Wodnicka et al., 2008; Carmona et al., 2009). By themselves, Ras superfamily proteins are small G proteins that cycle between inactive GDP-bound forms and active GTP-bound forms (Bourne et al., 1990). Exchange for GTP and hydrolysis of GTP to GDP are catalyzed by guanine nucleotide exchange factors and GTPase-activating proteins, respectively (Gloerich and Bos, 2011).

Another set of molecules that are increasingly recognized to play an active role in cell migration and tumor vascularization are ion channels, through changes in their expression and/or activity (Schwab et al., 2012; Fiorio Pla and Munaron, 2014). In this context, the discovery of the transient receptor poten-

*T. Genova and G.P. Grolez contributed equally to this paper.

**N. Prevarskaya, D. Gkika, and A. Fiorio Pla contributed equally to this paper.

Correspondence to Alessandra Fiorio Pla: alessandra.fiorio@unito.it

Abbreviations used: BTEC, breast tumor-derived endothelial cells; CPM, cellular Potts model; EC, endothelial cell; FN, fibronectin; HMEC, human microvascular endothelial cell; HUAEC, human umbilical artery endothelial cell; HUVEC, human umbilical vein endothelial cell; PLA, proximity ligation assay; PM, plasma membrane; PSA, prostate-specific antigen; Rap, Ras-associated protein; ROI, region of interest; TRP, transient receptor potential.

The Rockefeller University Press
J. Cell Biol. Vol. 216 No. 7 2107–2130
https://doi.org/10.1083/jcb.201506024

tial (TRP) superfamily of channels has provided candidates for nonvoltage gated Ca^{2+} entry mechanisms and their participation in different cellular processes. During the past 20 years, numerous studies have indicated that the expression and/or activity of TRP channels are in fact altered in cancers. In particular, the presence of the TRPC, TRPM, and TRPV subfamilies is correlated with malignant growth and cancer progression (Gkika and Prevarskaya, 2009; Prevarskaya et al., 2010). As such, TRP channels have been proposed as biomarkers for the diagnosis or prognosis of cancer progression, and targeting TRP channels has been suggested as a novel therapeutic strategy (Thebault et al., 2006; Nilius, 2007; Ding et al., 2010; Gkika and Prevarskaya, 2011). TRP channels are expressed in ECs, and their functions have been related to critical steps of tumor vascularization, such as cell migration and in vitro angiogenesis (Fiorio Pla et al., 2012a; Fiorio Pla and Gkika, 2013). In this regard, we unveiled how TRPV4 is overexpressed in tumor-derived ECs, in which it plays a key role in the control of cell migration (Fiorio Pla et al., 2012b). Moreover, increasing evidence demonstrates that ion channels are indeed pivotal regulators of directed cell migration. For example, Tsai et al. (2014) have recently proposed an integrated model of the spatial organization of the STIM1–ORAI1 signaling system, which dynamically controls the polarization and persistence of migration as well as local adhesion and turning, together with the actin regulators Rac, Cdc42, RhoA, and PtdIns (3;4;5)P3.

Among TRP channels, the cold/menthol–sensitive TRPM8 (belonging to the melastatin TRP subfamily) has emerged as an important player in cell migration and tumor progression; its expression is strongly up-regulated in prostate, breast, colon, lung, pancreatic, and skin cancers. In contrast, TRPM8 expression is dramatically reduced during late cancer stages and during metastatic dissemination in androgen-independent prostate cancer (Tsavaler et al., 2001; Henshall et al., 2003; Gkika and Prevarskaya, 2009; Yee et al., 2010; Grolez and Gkika, 2016). It has recently been proposed that TRPM8 could have a protective function in metastatic prostate cancer by impairing the motility of these cancer cells (Gkika et al., 2010, 2015). Conversely, apart from a very few studies suggesting TRPM8 expression in vascular cells (Johnson et al., 2009; Mergler et al., 2013; Sun et al., 2014), no information is available regarding its possible expression in tumor-derived ECs and its involvement in EC migration.

Here, we investigated the role of the TRPM8 channel in ECs and demonstrate that it inhibits EC adhesion, migration, spheroid sprouting in vitro, and self-assembly into a vascular network via a novel and completely unexpected role as a Rap1 GTPase inhibitor that controls β1-integrin–mediated EC behavior.

Results

Endogenous TRPM8 is expressed in ECs

TRPM8 expression was investigated in different types of ECs, namely human umbilical vein ECs (HUVECs), human umbilical artery ECs (HUAECs), human microvascular ECs (HMECs), and human breast tumor-derived ECs (BTECs). A single major band of 95–100 kD was detected in all EC types tested (Fig. 1 Ai), consistent with previously reported intracellular TRPM8 (Bidaux et al., 2007; Wondergem et al., 2008). As expected, the classic 130-kD TRPM8 form was clearly present in positive-control lysates obtained from HEK-293 cells with inducible TRPM8 expression (HEK-TRPM8 cells; Bidaux et al., 2007) but absent in ECs (Fig. 1 Bi). The intracellular localization of TRPM8 protein in ECs was confirmed by means of cell surface biotinylation assays; no TRPM8 expression was detected in the biotinylated surface fraction of ECs in the presence or absence of 10 µM of specific agonist icilin (for 10 min) when compared with HEK-TRPM8 cells used as positive controls, whereas TRPM8 was equally expressed in total cell lysates of both HMECs and HEK-TRPM8 cells (Figs. 1 Bi and S1 A). Similarly, confocal immunofluorescence analyses showed the colocalization of endogenous TRPM8 with the ER marker calnexin (Fig. 1 Bii). Interestingly, BTECs showed lower TRPM8 mRNA and protein levels than normal ECs (Fig. 1 Aii), further confirming the different expression pattern of Ca^{2+}-related proteins in BTECs compared with normal ECs (Fiorio Pla et al., 2008, 2010, 2012b; Pupo et al., 2011).

Constitutive TRPM8 inhibits EC migration, in vitro sprouting, and in vitro vascular network formation independently of channel pore function

Having assessed the presence of TRPM8 in ECs, we next investigated the possible role of TRPM8 in the control of the formation of capillary-like structures and vascular networks by cultured ECs. To this end, we first studied EC migration by means of wound-healing assays. HMEC and HUVEC stimulation with 10 µM icilin or 250 µM menthol progressively decreased their migration rate, with this difference becoming significant starting at 4 h (Fig. 1, Ci and Cii; and Fig. S1 Bi). No significant effect was detected in BTECs (Fig. 1 Cii) in accordance with the low levels of TRPM8 expression in this EC type. We previously described the role of prostate-specific antigen (PSA) as an endogenous TRPM8 activator responsible for prostate cancer inhibition of cell migration (Gkika et al., 2010). We therefore studied here the role of PSA in EC migration to test the hypothesis of a common endogenous regulator of TRPM8-mediated cell migration. Indeed, 40 ng/ml PSA treatment significantly reduced EC migration starting from 4 h similarly to 10 µM icilin treatment (Fig. 1, Ci and Ciii).

To confirm the role of endogenous TRPM8 in modulating EC migration, we repeated wound-healing assays after the specific silencing of the channel using siRNAs in both HMEC and HUVECs. After 72 h of transfection, TRPM8 silencing was monitored at the protein level by immunoblot analysis, and found to be significantly decreased in HMEC and HUVECs (by 60% and 50%, respectively; Fig. S1 C). Interestingly, silencing of endogenous TRPM8 in ECs was sufficient to promote a significant increase in the migration rate in both HMECs and HUV ECs starting from, respectively 4 h or 6 h, suggesting a basal role of the channel in the control of EC migration (Fig. 2 A). Consistent with these results, TRPM8 overexpression in BTECs significantly inhibited cell migration even in the absence of 10 µM icilin (Fig. 2 B).

We next investigated the effective role of ion fluxes generated by TRPM8 on cell migration. For this purpose we performed wound-healing experiments overexpressing a TRPM8 construct that carry a single point mutations in TRPM8 pore region (Y905A) which completely inhibits channel activity as recently characterized (Bidaux et al., 2015). Interestingly, when transfecting BTECs with $TRPM8^{Y905A}$, EC migration was significantly inhibited, even in the absence of channel agonist, to

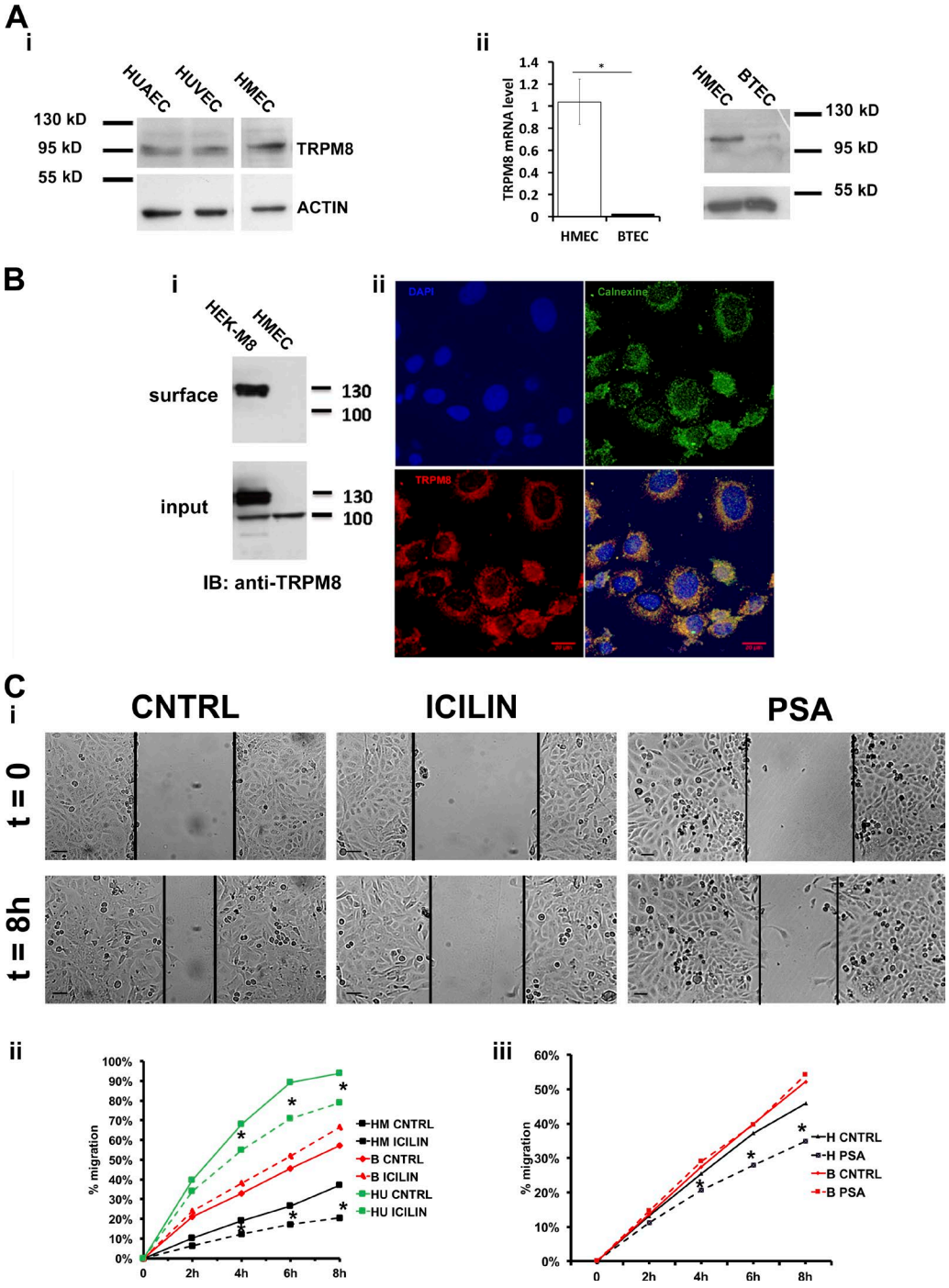

Figure 1. **TRPM8 is endogenously expressed in EC and its stimulation inhibits cell migration.** (Ai) Western blot analysis of TRPM8 protein levels in HMECs, HUVECs, and HUAECs. (Aii) Analysis of TRPM8 mRNA expression by qPCR levels and protein expression in HMECs and BTECs. For quantitative PCR, data were normalized to 18S rRNA. Data are mean ± SEM of three different experiments. (B) TRPM8 in HMECs is expressed on the ER. (Bi) Surface biotinylation experiment performed on HMECs and HEK cells overexpressing TRPM8 (HEK-TRPM8 cells). (Bii) Representative confocal images of HMECs showing DAPI staining (blue), calnexin (green), and TRPM8 (red) immunolabeling; the merged image shows the colocalization of endogenous TRPM8 with calnexin, indicating intracellular TRPM8 localization. (C) TRPM8 stimulation inhibits the migration of normal, but not tumor, ECs. (Ci) Representative photographs of a wound-healing assay performed on HMECs treated with control medium, 10 μM icilin, or 40 ng/ml PSA taken at two different time points (t = 0 h, top; t = 8 h, bottom). Bars, 50 μm. (Cii) Plot of the percentage of migration of BTECs (red), HMECs (black), and HUVEC (green) under control conditions (growth medium) or treated with 10 μM icilin. (Ciii) Plot of the percentage of migration of BTECs (B in red) and HMECs (H in black) under control conditions (growth medium) or treated with 40 ng/ml PSA. *, $P < 0.05$ for comparisons between cells of the same type treated with or without icilin (Cii) or PSA (Ciii).

an extent similar to wild-type TRPM8 overexpression (Fig. 2, Bi and Bii). These data demonstrate that the biological effects of TRPM8 on EC migration described here are not imputable to the pore function of the TRPM8 protein.

To further investigate the biological roles of TRPM8 in ECs, we studied in vitro vascular tubulogenesis by exploiting the permissive properties of Matrigel. In icilin- or menthol-stimulated ECs, we observed a strong reduction in their ability

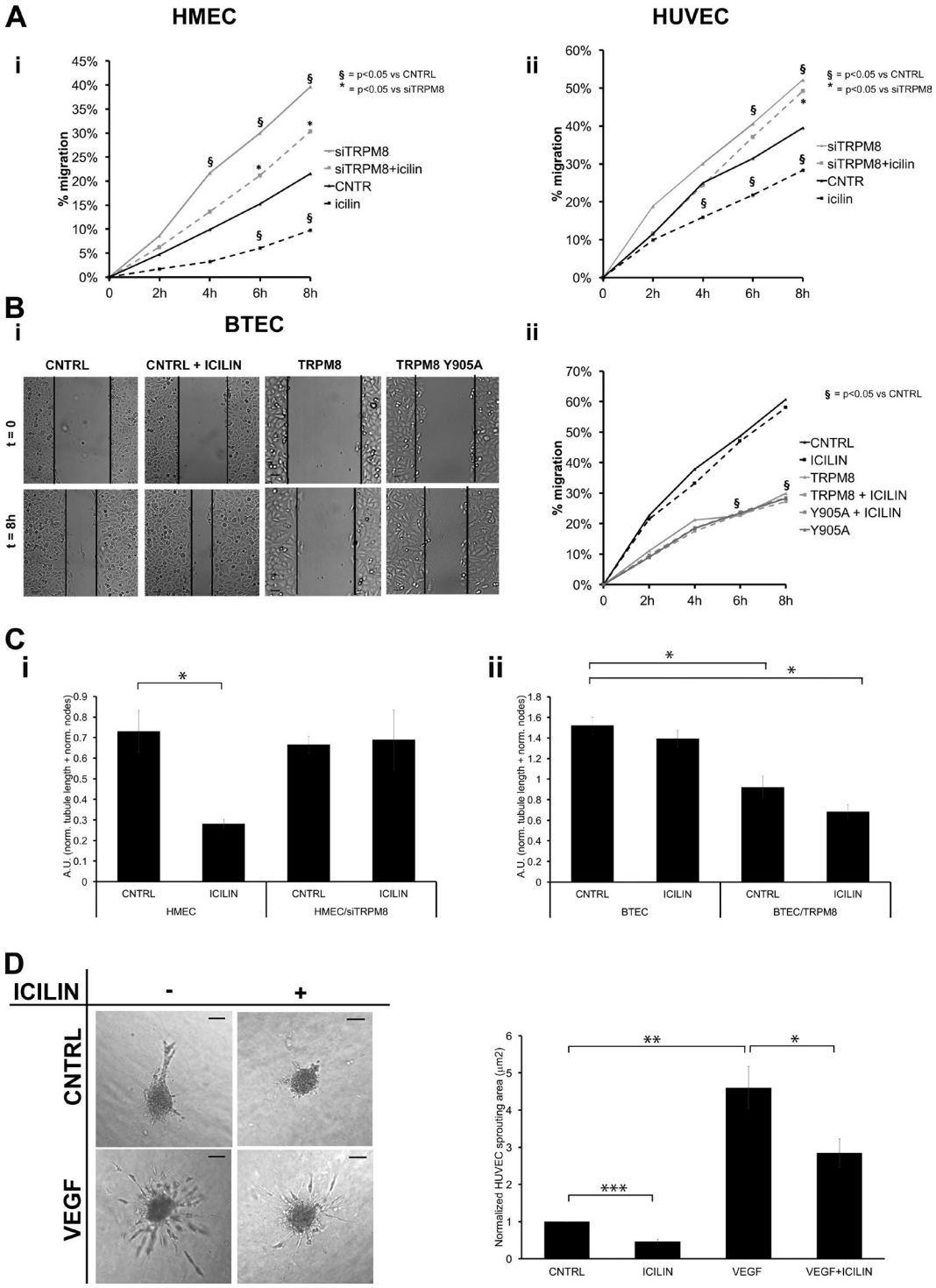

Figure 2. **TRPM8 inhibits EC migration independently of the channel's pore function.** (Ai) Plot of the percentage of migration in the wound area of silenced HMECs (siTRPM8 in gray and CNTRL in black). (Aii) Plot of the percentage of migration in the wound area of silenced HUVECs (siTRPM8 in gray and CNTRL in black). (Bi) Representative photographs of a wound-healing assay taken at two different time points (t = 0 h, top; t = 8 h, bottom). BTECs transfected with 2 µg of a GFP control vector (CNTRL), 2 µg TRPM8, or TRPM8^{Y905A} were treated with control medium or 10 µM icilin. Bars, 50 µm. (Bii) Plot of the percentage of migration of BTECs overexpressing TRPM8 (TRPM8, in gray) TRPM8^{Y905A} (TRPM8^{Y905A}, in red; TRPM8^{Y905A} + icilin, in green) or GFP as a control (CNTRL, in black). §, significant difference relative to control. (C) TRPM8 inhibits in vitro vascular network formation. (Ci) Quantification of tubulogenesis in HMECs silenced for TRPM8 (HMEC/siTRPM8) or not (HMECs). (Cii) Quantification of tubulogenesis of BTECs overexpressing TRPM8 (BTEC/TRPM8) or not (BTECs). *, $P < 0.05$. (D) TRPM8 inhibits EC in vitro sprouting. Representative bright-field micrographs of control (CNTRL) or VEGF-stimulated (VEGF) EC spheroids, in the presence or absence of 10 µM icilin showing reduced vascular sprouting in spheroids. Bars, 50 µm. The bar graphs show quantification of EC spheroid sprouting area, revealing that stimulation of TRPM8 by icilin reduced the sprouting area. Data are expressed as mean ± SEM. *, $P \leq 0.05$; **, $P \leq 0.01$; ***, $P \leq 0.001$.

to self-assemble into interconnected tubules in Matrigel, which was prevented by TRPM8 silencing (Figs. 2 Ci and S2 B). Conversely, and as expected, icilin treatment did not affect the ability of BTECs to form vascular networks. Remarkably, TRPM8 overexpression in BTECs promoted a substantial reduction in tubule formation, even in the absence of external activators, suggesting a basal role of the channel in the control of both EC migration and in vitro vascular morphogenesis (Figs. 2 Ciii and S2 B). Notably, exogenous TRPM8 is likely localized at both the intracellular and PM levels, as also confirmed by Ca^{2+} imaging and electrophysiological recordings (Fig. S4, A and B).

Finally, to study the role of TRPM8 on vessel sprouting, we performed HUVEC spheroid sprouting assays. TRPM8 is critically involved in in vitro EC sprouting, as icilin treatment significantly decreased the sprouting area after 24 h treatment, both in the basal condition and in VEGF-stimulated spheroids ($n = 60$ spheroids per experimental condition; Fig. 2 D).

TRPM8 inhibits EC adhesion

The dynamic control of cell-to-ECM adhesion is a fundamental aspect of EC migration and vascular morphogenesis (Serini et al., 2006; Francavilla et al., 2009). We therefore tested the hypothesis that the inhibition of EC migration by TRPM8 could be caused by an impairment in the ability of cells to adhere to the ECM. We acutely treated adherent ECs with 10 µM icilin and, using time-lapse video microscopy, we observed that 77% of the analyzed cells immediately rounded up upon TRPM8 activation ($n = 52$ cells; Fig. 3 Ai). To better quantify this effect, we took advantage of an impedentiometric system that can monitor over time the spread of cultured cells using electrical impedance as a readout. We found that, compared with untreated control conditions, icilin stimulation reduced EC adhesion and area of spread, with a peak effect at 10 min of treatment (Fig. 3 Aii); subsequently, ECs began to respreads, although they still displayed lower adhesion and spread compared with untreated control ECs (Fig. 3 Aii, inset graph).

This cell rounding-up effect was supported by a multiscale hybrid mathematical approach (Fig. S3, A and B) based on the cellular Potts model (CPM) framework (Graner and Glazier, 1992; Glazier and Graner, 1993; Scianna et al., 2013), which allows the description of cell adhesion and migration as well as the underlying molecular dynamics to be described. As shown in Fig. 3 B, the results of the mathematical simulation were in agreement with "wet" experiments, displaying a similar shrinkage effect in the presence of the TRPM8 agonist icilin (Fig. 3 Bi). Remarkably we observed that basal TRPM8 channels in the absence of external agonist was sufficient to promote a rounding-up effect in virtual cells in the mathematical model (Fig. 3 Bii). The model also confirmed that TRPM8 expression significantly reduced cell migration speed and random cell velocity, in accordance with the aforementioned migration assays (Fig. S3 C).

Model prediction of TRPM8 cellular location

Taking advantage of the flexibility of our mathematical approach, we decided to further characterize the significance of the subcellular localization of TRPM8 for its function. Although TRPM8 in ECs is intracellular, localization at the plasma membrane (PM) has also often been described. We simulated the selective localization of TRPM8 either in intracellular compartments (ER) or at the PM. Notably, mathematical model predictions showed that when TRPM8 was exclusively localized at the PM, cell migration speed was strongly inhibited, to an extent largely identical to that observed when TRPM8 was localized exclusively at the ER (Fig. S3 D). We then simulated different levels and different ER/PM ratios of TRPM8 expression. Interestingly, the modeled outcomes clearly predict that cell behavior is significantly affected by the overall level of TRPM8, but not by its subcellular localization. In fact, as indicated in Fig. S3, variations in the ER/PM ratio did not significantly alter cell migratory determinants. It should be noted that the in silico approach allows the subcellular localization of TRPM8 to be precisely defined, something that cannot be achieved in living cells, in which a fraction of the channel is likely trapped in the ER at all times. However, the results obtained by our mathematical approach were supported by cell migration assays performed under comparable experimental conditions, i.e., with HMECs that did not express any detectable TRPM8 at the PM (Figs. 1 C and 2 A) and with BTECs in which TRPM8 was overexpressed (Fig. 2 B) and likely localized both at the intracellular and PM levels, as also confirmed by the transient and sustained phase in Ca^{2+} imaging experiments and electrophysiological recordings in the latter cells (Fig. S4, A and B).

TRPM8 inhibits EC adhesion by negatively interfering with inside-out β1-integrin signaling

To better characterize the molecular mechanisms by which TRPM8 controls EC adhesion to the ECM, we next performed adhesion assays on ECs seeded on increasing concentrations of FN. There was a progressive increase in the number of adherent cells with increasing FN concentrations, suggesting a role for α5β1 integrin in EC adhesion (Figs. 3 C and S5 A). Moreover, icilin stimulation promoted a substantial reduction of EC adhesion to FN, regardless of the concentration of the latter (Figs. 3 C and S5 A); similar results were obtained in the presence of menthol (Fig. S1 Biii). To substantiate the role of α5β1 integrin in TRPM8-mediated EC inhibition, we next performed haptotaxis assays, in which ECs were induced to directionally migrate toward surface-bound 1 µg/ml FN; TRPM8 stimulation did not have any effect on EC migration in the absence of the surface-bound haptotactic stimulus but significantly inhibited it in the presence of FN (Figs. 3 D and S5 B).

The specificity of TRPM8 and its role in controlling cell-to-ECM adhesion was further assessed by specific channel silencing, which prevented the icilin-driven inhibition of HMEC or primary HUVEC adhesion to FN (Fig. 3, E and F; and Fig. S5, C and D). Conversely, TRPM8 overexpression in BTECs (Figs. 3 G and S5 E) or even in HMECs (Fig. S4 C) significantly reduced the relative percentage of adherent cells to FN, with or without icilin treatment.

To directly verify the involvement of β1-integrin in the TRPM8-mediated signaling pathway, we performed adhesion assays in the presence of the β1-integrin antibody 9EG7 that recognizes and stabilize active β1-integrins (Lenter et al., 1993; Bazzoni et al., 1995). The addition of 9EG7 fully reversed TRPM8-mediated inhibition of relative percentage of adherent ECs to FN (Figs. 4 A and S5 F). These results clearly show that TRPM8 modulates EC adhesion to FN through the inactivation of its major receptor, namely α5β1 integrin. Moreover, the rescue effect observed upon 9EG7-elicited β1-integrin activation indicates that TRPM8 effect in EC adhesion is likely caused by an inhibitory effect on the inside-out signaling pathways

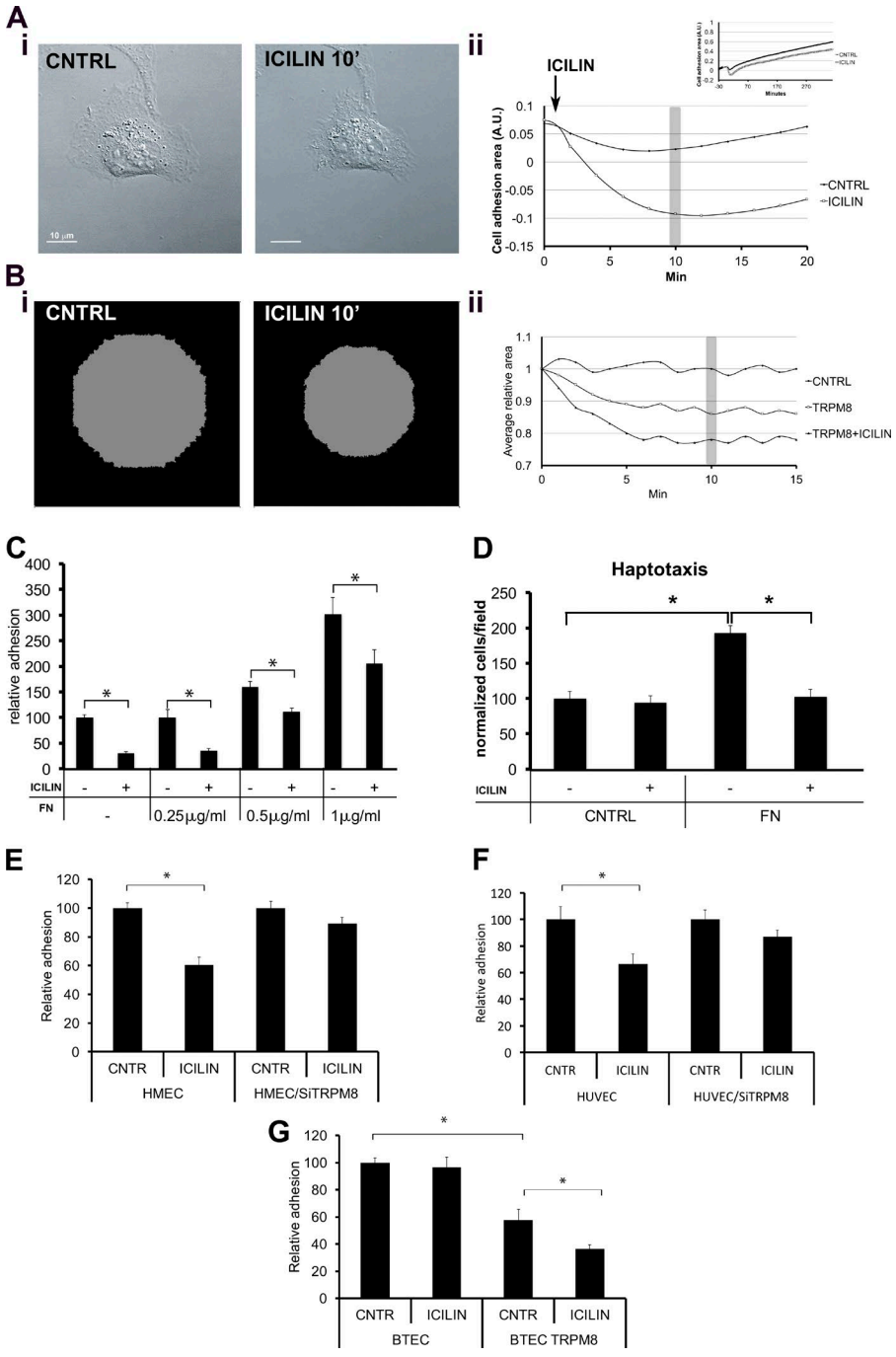

Figure 3. **TRPM8 stimulation inhibits cell adhesion.** (Ai) Representative photographs showing the "rounding-up" effect induced by treatment with icilin for 10 min (right). (Aii) Quantification of cell adhesion area in HMECs treated with icilin (white circles) or not (black circles) and plated on FN. The experiment was performed using the XCelllgence-Roche apparatus. The gray bar indicates values relative to the stage represented in Ai. (Bi) Simulation of the rounding-up effect in a virtual cell expressing basal levels of 0.2 µM TRPM8, treated with icilin. (Bii) Evolution in time of the relative area of a simulated cell depleted of TRPM8 (CNTRL) or expressing basal levels of TRPM8 and treated with icilin (TRPM8+icilin) or not (TRPM8). The gray bar indicates values relative to the stage represented in Bi. (C) Quantification of adherent HMECs treated or not with 10 µM icilin on plates coated with 0, 0.25, 0.5, and 1.0 µg/ml FN. *, $P < 0.05$. (D) Quantification of haptotaxis of HMECs treated or not with 10 µM icilin on 1 µg/ml FN or control substrate. *, $P < 0.05$. (E) Quantification of adhesion to FN of HMECs silenced for TRPM8 (HMEC/siTRPM8) or not (HMEC), in the presence or absence of icilin. (F) Quantification of adhesion to FN of HUVECs silenced for TRPM8 (HUVEC/siTRPM8) or not (HUV EC), in the presence or absence of icilin. (G) Quantification of adhesion to FN of BTECs overexpressing TRPM8 (BTEC/TRPM8) or not (BTEC), in the presence or absence of icilin. *, $P < 0.05$. All data in C–G represent adhesion normalized to the control untreated condition. Data are expressed as mean ± SEM.

that control integrin activation. To better test this hypothesis, the activity of β1-integrin was evaluated in HUVECs by means of immunofluorescence staining 9EG7 antibody for active β1-integrins. TRPM8 stimulation with 10 µM icilin clearly and significantly inhibited the 9EG7 distribution in HUVECs, with a maximal effect after 30 min treatment ($n = 15$ cells per experimental condition; Fig. 4 C).

The involvement of FAK, a key downstream effector of β1-integrin–driven cell adhesion and migration, was evaluated by Western blot analysis. Compared with control ECs, stimulation of TRPM8 by 10 µM icilin promoted a significant reduction in FAK autophosphorylation at the predominant Tyr 397 phosphorylation site (Fig. 4 B).

Rap1 interacts with TRPM8 in ECs

Because our data suggested that TRPM8 could inhibit EC adhesion to FN by impinging on the inside-out signaling pathways that promote integrin activation, we next decided to determine the molecular mechanisms responsible for this inhibition. Immunoprecipitation experiments did not show a convincing or robust interaction between endogenous or exogenous TRPM8 and β1-integrins, suggesting the possible involvement of an intermediate molecule. We therefore took advantage of a GST pull-down assay using TRPM8 cytosolic tails as bait on lysates of healthy mouse prostates to screen for candidate proteins interacting with TRPM8 (for the full list of candidates, see Gkika et al., 2015).

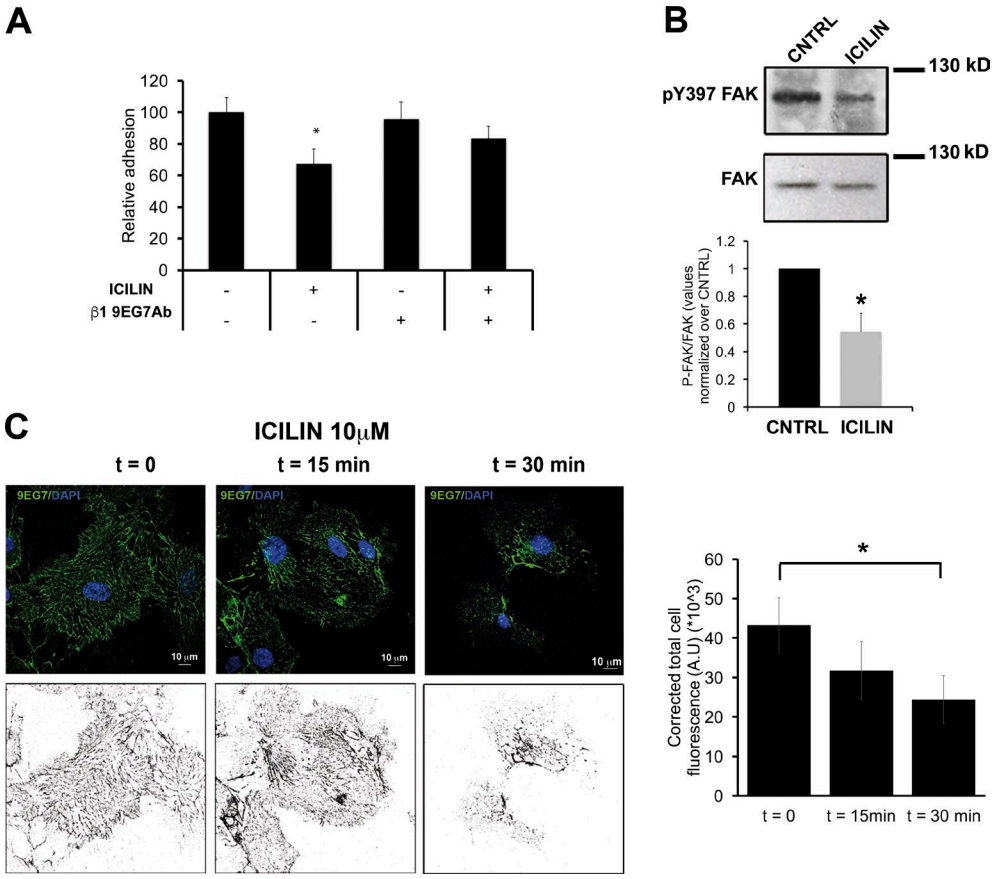

Figure 4. **TRPM8 inhibits EC adhesion through the Rap1–integrin–FAK pathway.** (A) TRPM8 acts through the α5β1 integrin signaling pathway. Quantification of adhesion to FN of HMECs treated (or not) with icilin, the integrin-activating 9EG7 antibody both in the presence of 0.1 mM $MnCl_2$. Data represent adhesion normalized to the control untreated condition. (B) Western blot analysis of phosphorylated FAK (pY397 FAK) and total FAK protein levels in HMECs treated or not with 10 µM icilin for 10 min. Quantification of normalized pY397-FAK/FAK protein levels in HMECs from three independent experiments (bottom). (A and B) *, $P < 0.05$ (Wilcoxon–Mann-Whitney test). (C) Representative images showing anti–β1-integrin antibody 9EG7 (green) and DAPI (blue) in HUVECs stimulated with for 15 or 30 min or untreated cells (t = 0). The bottom panel represents the same images binarized to better underlie the active β1-integrin organization. Bar graph on the right shows quantification of the corrected total cell fluorescence. Data are expressed as mean ± SEM. *, $P \leq 0.05$ (two-tailed heteroscedastic Student's *t* test).

Among the proteins interacting with TRPM8, our interest was drawn by Rap1, a small GTPase that is well known for its role as an effective integrin activator (Reedquist et al., 2000; Lafuente et al., 2004; Chrzanowska-Wodnicka et al., 2008; Carmona et al., 2009). Importantly, we confirmed the interaction between TRPM8 and Rap1 in intact cells by transiently expressing and then immunoprecipitating an HA-tagged wild-type Rap1 (Rap1-WT) in inducible HEK-TRPM8 cells (Figs. 5 A and S6 A). Similarly, Rap1-WT immunoprecipitated with $TRPM8^{Y905A}$ pore mutant proteins (Fig. 5 A), suggesting TRPM8 pore activity is not crucial for the interaction between the two proteins. We additionally studied the physical interaction between the endogenous TRPM8 and Rap1 and moreover localized the protein interaction complexes at the cellular level. We used the proximity ligation assay (PLA), which can detect protein–protein binding in situ at single-molecule resolution. PLA for Rap1:TRPM8 produced abundant red puncta in HMECs that doubled upon treatment with icilin (Fig. 5 B), suggesting a stronger Rap1 :TRPM8 interaction. In addition, in HMECs activated or not with icilin, siRNA against TRPM8 significantly decreased the puncta abundance, validating the specificity of the assay (*n = 85* cells for control, *n* = 83 cells for the icilin treatment, and for the siTRPM8 the cell numbers were *n* = 91 and *n* = 93, respectively). No puncta were detected in control conditions (Fig. S5 G).

Further, to investigate which TRPM8 cytosolic tail is interacting with Rap1, we produced and purified the TRPM8 N-terminal tail and C-terminal tail fused to GST (Fig. 5 C, inset). Pull-down of the GST-fused termini of TRPM8 with lysates of HEK cells overexpressing GFP-tagged Rap1-WT showed interaction of Rap1-WT mainly with the TRPM8 N-terminal tail and to a lesser extent with the TRPM8 C-terminal tail, whereas no interaction was observed with GST alone (Figs. 5 C and S6 B, left).

TRPM8 activation retains Rap1 intracellularly, preventing its cytoplasm-PM trafficking

Given that TRPM8 and Rap1 interact, we next evaluated the dynamics of the TRPM8–Rap1 interaction in living ECs by means of confocal time-lapse recordings of ECs expressing GFP-Rap1-WT, TRPM8-YFP, and the ER marker ER-DsRed. In accordance with previously reported data (Bivona et al., 2004; Carmona et al., 2009), GFP-Rap1-WT partially accumulated at the PM, in particular at the leading edge of migrating ECs (Fig. 6 A). In contrast, TRPM8-YFP was localized in close proximity to ER-DsRed, similar to what was observed with endogenous TRPM8 expression (Fig. 1 B).

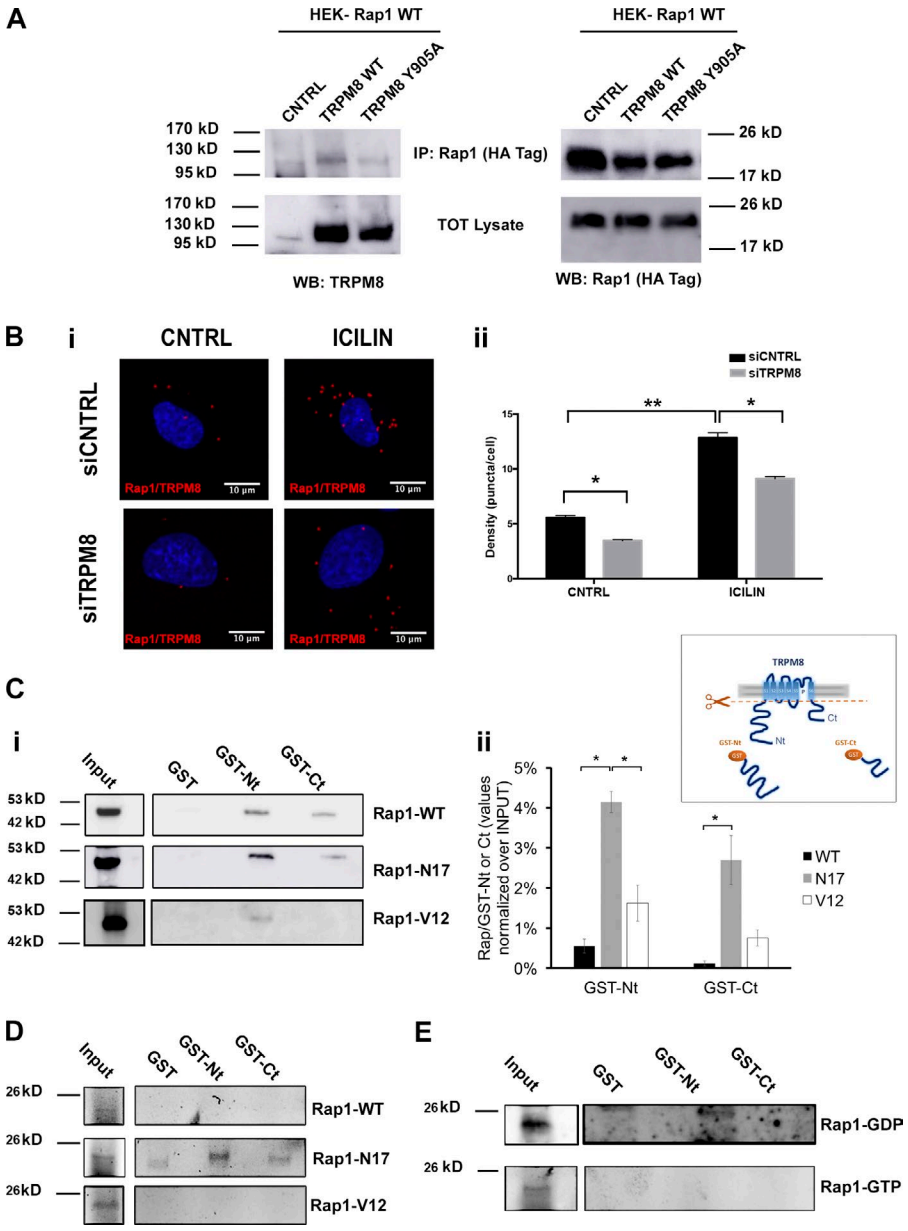

Figure 5. **Rap1 is a TRPM8-interacting protein.** (A) Representative immunoprecipitation experiments. Expression vectors encoding Rap1-WT-HA were transfected into HEK-overexpressing TRPM8- or TRPM8^{Y905A}-tagged cells. Cell lysates were immunoprecipitated (IP) with an anti–HA antibody and immunoblotted with antibodies against TRPM8 and HA. Images in C and D are representative of three independent experiments. (B) In situ detection of endogenous TRPM8/Rap1 interaction in HMECs. TRPM8/Rap1 complexes were monitored using PLA using anti–TRPM8 and Rap1 antibodies followed by staining with proximity probes, ligation, and localized rolling-circle amplification. HMECs silenced for TRPM8 (siTRPM8) or not (siCNTRL), in the presence or absence of 10 µM icilin (10 min treatment). Close locations between the two proteins were observed as red fluorescent dots and DAPI-stained nuclei as blue. (Bii) Puncta density quantified as mean ± SEM puncta per cell. *, $P \leq 0.05$; **, $P \leq 0.001$ (Student's *t* test). (Ci) TRPM8 N-terminal tail (GST-Nt), C-terminal tail (GST-Ct), or GST were incubated with lysates of HEK cells overexpressing Rap1-WT-GFP, Rap1-N17-GFP, or Rap1-V12 and precipitated using GST. Western blotting was performed with anti–GFP antibody. One representative experiment of three is shown. (Cii) Quantification of Rap1/TRPM8 tails normalized over the input. Data are expressed as mean ± SEM. *, $P < 0.05$ (Student's *t* test). Inset shows a scheme representing GST-Nt and C-terminal tail purification. (D) GST pull-down assay of in vitro translated Rap1WT, Rap1-N17, or Rap1-V12 using FluoroTect and GST or GST fused to the GST-Nt or GST-Ct. 10% of the in vitro translated Rap1 were used for the input of the GST pull-down (top). Bodipy-FL-stained gel are shown for the expression of Rap1. (E) The GST pull-down assay was repeated by loading in vitro translated RAP1-WT with 1 mM GDP (left) or 0.1 mM GTP (right). Anti-GST or anti–Rap1 antibodies were used to visualize the interaction of Rap with GST-fused N- and C-terminal tail. All the gels are representative of at least three independent experiments.

The stimulation of migrating ECs with 10 µM icilin promoted a massive change in the subcellular localization of GFP-Rap1-WT characterized by its strong retention in close proximity to ER-localized TRPM8-YFP (Fig. 6 Aiii; $n = 5$ cells). To quantify this retention effect, we measured the distance between GFP-Rap1-WT and TRPM8-YFP or ER-DsRed fluorescent signals, calculated from each plot profiles (see Materials and methods). Both Rap1-WT/ER and Rap1-WT/TRPM8 distances significantly diminished starting 4 min after icilin application (Fig. 6, Bi and Bii, respectively, red and blue bars). Furthermore, the distance between GFP-Rap1-WT and the PM significantly increased during the same time period, thus confirming the intracellular retention of GFP-Rap1-WT (Fig. 6, Biii and Biv, black bars). As a consequence of the intracellular retention, ECs rounded up, decreasing the area they occupied, as shown by the reduction in GFP-Rap1-WT/PM distance at later time points (Fig. 6 Biv, black bars), in accordance with the rounding-up effect induced by TRPM8 stimulation (Fig. 3 A). Interestingly, GFP-Rap1-WT retention preceded the rounding-up effect (Fig. 6 Biv), suggesting that the latter could be functionally correlated with the loss of Rap1-WT-GFP from the PM.

To evaluate whether GFP-Rap1-WT retention was mediated by endogenous TRPM8, we then performed time-lapse confocal analyses of live ECs in which TRPM8 was silenced using siRNAs. As expected, GFP-Rap1-WT was retained intracellularly after icilin stimulation in control ECs ($n = 7/7$ cells; Fig. 7, siCNTRL) whereas no significant effect was observed after icilin treatment in TRPM8-silenced ECs, in which GFP-Rap1-WT continued to be largely associated with the PM ($n = 7/8$ cells; Fig. 7, siTRPM8).

TRPM8 activation inhibits Rap1 activity by sequestering inactive Rap1

To study the endogenous activity of Rap1 on ECs, we performed a new set of live-cell GTPase activity assays using the GFP-RBD$_{RalGDS}$ probe, a GFP-based probe designed to reveal when and where in the cell specific GTPases become activated (GTP bound; Bivona et al., 2004; Bivona and Philips, 2005).

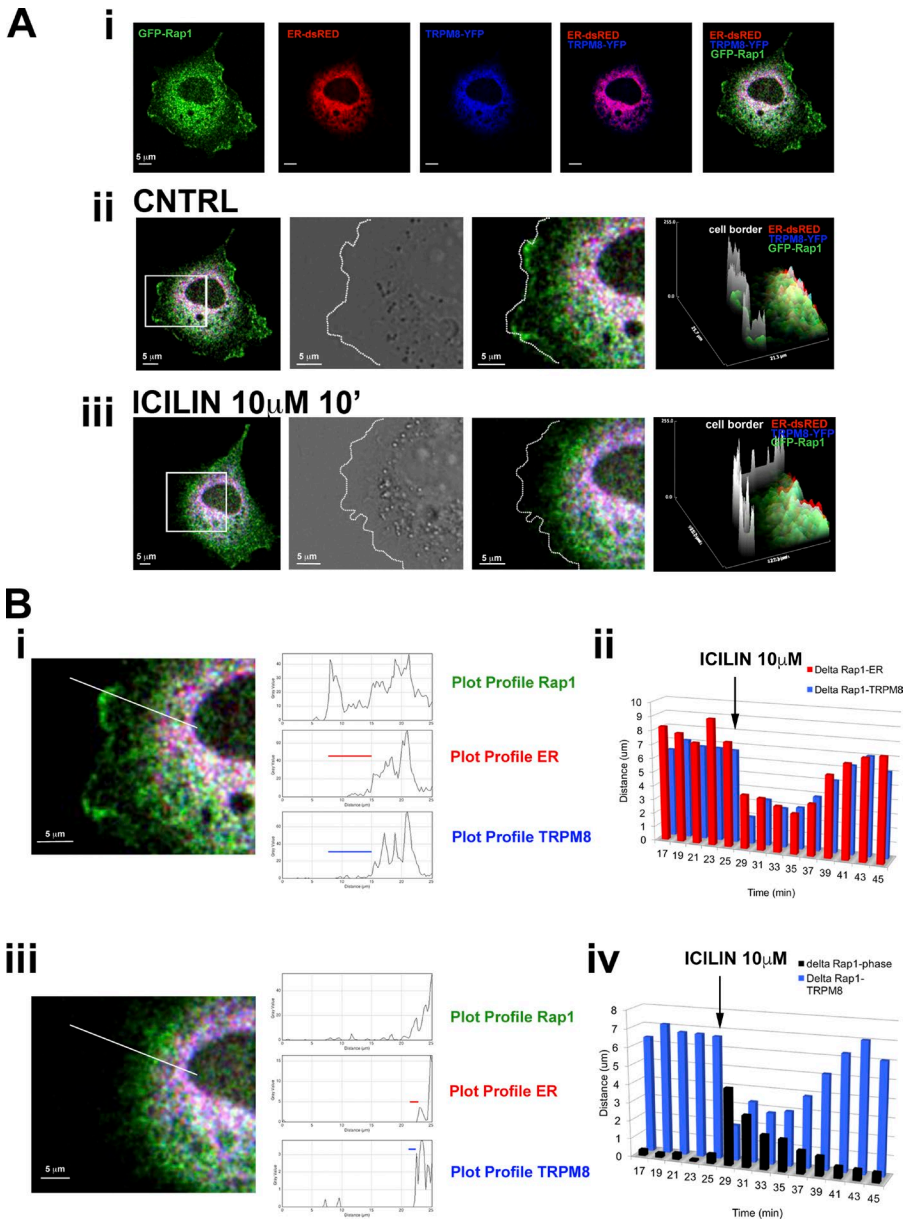

Figure 6. **TRPM8 activation leads to the internalization of Rap1.** (Ai) Representative confocal time-lapse analysis of HMECs transfected with 1 µg GFP-Rap1 (green), 2 µg TRPM8 (blue), and 1 µg ER-DsRed to label the ER (red). On the right, the merged images are shown. (Aii and Aiii) Enlargements of the PM interface region displaying the internalization effect of TRMP8 activation on Rap1. The PM is shown by the dotted line in gray. On the right, the surface plot analysis is shown. (Bi and Biii) Plot profile of Rap1, ER, and TRPM8 signals in HMECs under control conditions and after 10 min of treatment with 10 µM icilin. On the left is a photomicrograph of the cell in with a line indicating the cross section used for the plot profile. (Bii and Biv) Plots showing the means from a representative experiment of the distances measured between Rap1 and ER (red), between Rap1 and TRPM8 (blue), and between Rap1 and the PM (black) in HMECs under control conditions and after 10 min of treatment with 10 µM icilin. The distances were calculated as means of at least three different plot profiles for at least three regions of interest (cross sections) within each EC.

Spatiotemporal activation of endogenous Rap1 was studied in control and siTRPM8 transfected cells (Fig. 8 Ai). Membrane recruitment of GFP-RBD was quantified as direct indication for Rap1 activity caused by restricted localization of the active Rap1 pool at the PM; in particular, we measures the cytosolic retention fraction of GFP-RBD after icilin treatment (Bivona et al., 2004; Bivona and Philips, 2005; see also Materials and methods and Fig. S2 C). Our results clearly show that Rap1 activation at the PM is significantly decreasing in the presence of icilin treatment (n = 18 regions of interest [ROIs], 5 cells; Fig. 8 A, siCNTRL; and Video 1) However, no significant effect was observed after icilin treatment in TRPM8-silenced cells, in which GFP-RBD_{RalGDS} continued to be largely associated with the PM (n = 17 ROIs, 5 cells; Fig. 8 A, siTRPM8; and Video 2).

To investigate the functional effects of TRPM8 activation on Rap1 activity, we performed pull-down assays for GTP-bound Rap1 using GST-RalGDS, which binds active Rap1-GTP. Notably, after 10 µM icilin treatment, the amount of active Rap1-GTP protein present in HMECs significantly decreased by ~50% as compared with control untreated HMECs or primary HUVECs (Fig. 8 B). Rap1 activity in endogenous TRPM8 was confirmed by pull-down assays on control (Fig. 8 B, siCNTRL) or TRPM8-silenced ECs (siTRPM8; both HMECs and HUVECs), which did not show any significant Rap1-GTP decrease in the presence of 10 µM icilin treatment (Fig. 8 B). To study the effect of ion fluxes on Rap1 activity, we transfected HMECs with both TRPM8 or $TRPM8^{Y905A}$ pore mutant plasmids. Interestingly TRPM8 or $TRPM8^{Y905A}$ overexpression significantly inhibited Rap1 activity at an extent similar to that of icilin treatment on HMEC control conditions; moreover, further treatment with icilin did not promote any additional inhibition of Rap1 activity (Fig. 9, Ai and Aii). These data confirm the pore-independent role of TRPM8. The functional effect of PSA treatment on Rap1 activity was studied by pull-down assays for active GTP-bound Rap1 using GST-RalGDS. Similarly to 10 µM icilin treatment, 10-min treatment with 40 ng/ml PSA significantly reduced the amount of active GTP-bound Rap1 (Fig. 9 B). These results suggest a correlation between PSA

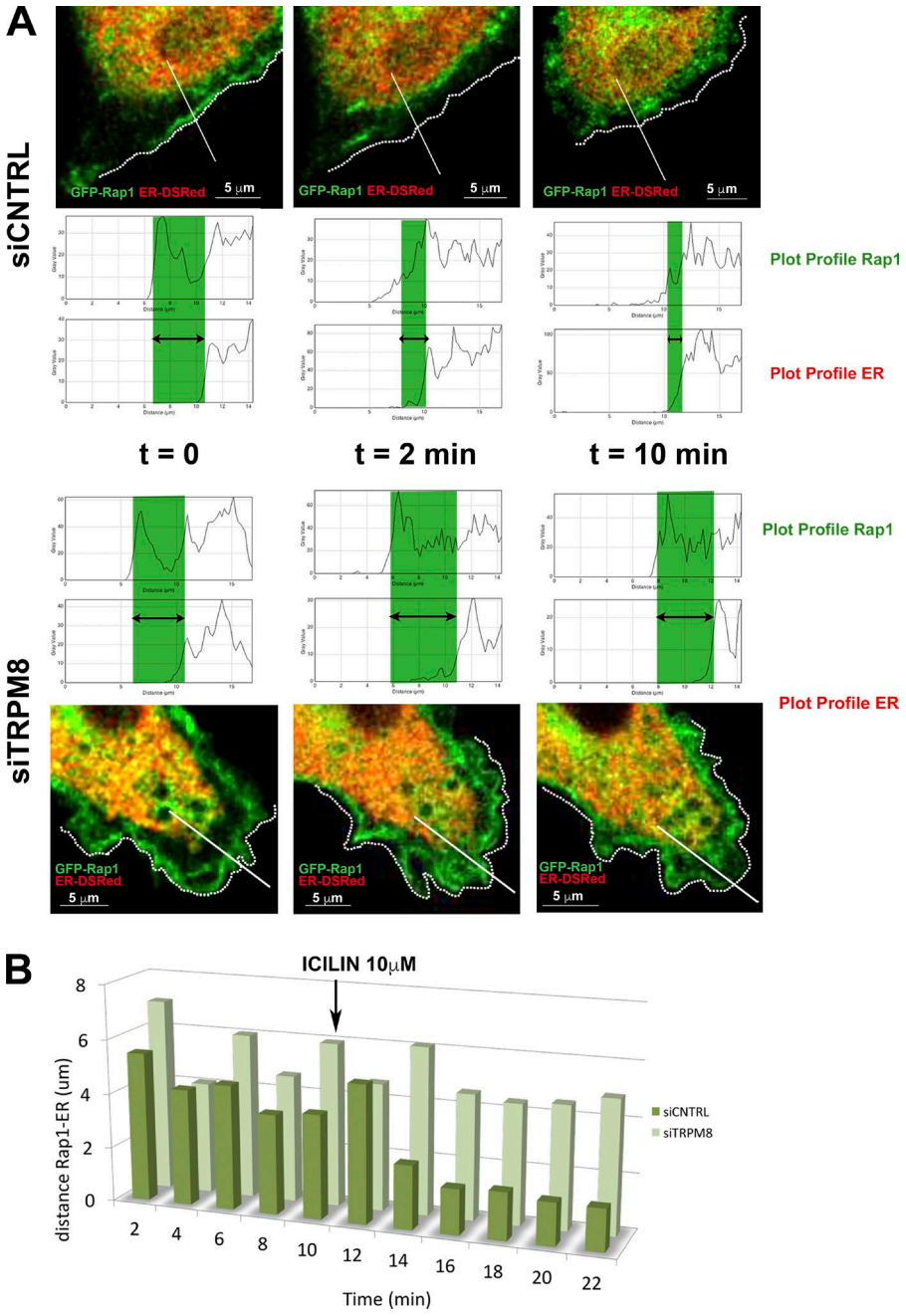

Figure 7. **Intracellular Rap1 retention is prevented by TRPM8 silencing in ECs.** (A) Live-cell imaging by confocal microscopy of ECs expressing GFP-Rap1 (green) and ER-DsRed (red) in control (siCNTRL) and siTRPM8-treated ECs (siTRPM8). Representative images showing Rap and ER dynamics in siCNTRL- and siTRPM8-treated ECs at t = 0 and after 2 or 10 min of treatment with 10 µM icilin; dotted white lines represent the PM. Representative plot profiles along the white lines in the images. The green bars depict the distance between the Rap1 and ER fluorescence signals. (B) Plot showing the means from a representative experiment of the distances measured between Rap1 and ER between Rap1 and TRPM8 in control (siCNTRL) and siTRPM8-treated ECs treatment with 10 µM icilin. The distances were calculated as means of at least three different plot profiles for at least three ROIs (cross sections) within each EC.

activity and TRPM8-mediated EC inhibition via Rap1, thus suggesting a possible role of PSA as an endogenous activator and common target for both cancer cells and ECs.

Interestingly, adhesion assays performed after transfecting ECs with increasing amounts of the inactive N17 mutant of Rap1 (van den Berghe et al., 1997; Reedquist et al., 2000) showed that the inhibitory effect of TRPM8 activation on the number of adherent ECs was completely prevented by Rap1-N17 in a dose-dependent manner (Fig. 9 D), whereas no significant effect was observed when transfecting cells with the constitutively active Rap1-V12 mutant (Fig. S4 D). Notably, Rap1-N17 did not affect the basal adhesion of ECs to FN, whereas a significant increase in adhesion was observed in ECs transfected with Rap1-V12 (Fig. S4 E), in accordance with the data on Jurkat cell adhesion (Reedquist et al., 2000). Moreover, reintroducing TRPM8 in the presence of Rap1-N17 rescued the inhibitory effect of icilin in cell adhesion; icilin is again in fact able to inhibit the EC number of adherent cells starting from TRPM8 transfection with 0.5 µg plasmid (Fig. 9 E). The mathematical model reproduced this behavior in terms of migration velocity by predicting a saturation effect at sufficiently high doses of Rap1-N17 and a rescue of the inhibitory effect of icilin by TRPM8 activation (Fig. 9, F and G).

Based on the aforementioned findings, we hypothesized that TRPM8 could act as Rap1 inhibitor, retaining the GDP-bound form of Rap1 and blocking its GDP-GTP exchange and normal ER–PM shuttling, thus resulting in the robust inhibition of Rap1 function. In the presence of an excess of Rap1-GDP (e.g., when Rap1-N17 is overexpressed in ECs), endogenous TRPM8 preferentially binds and sequesters it, allowing unbound endogenous Rap1 to become activated by exchanging GDP for GTP and thereby activating β1-integrin and resulting

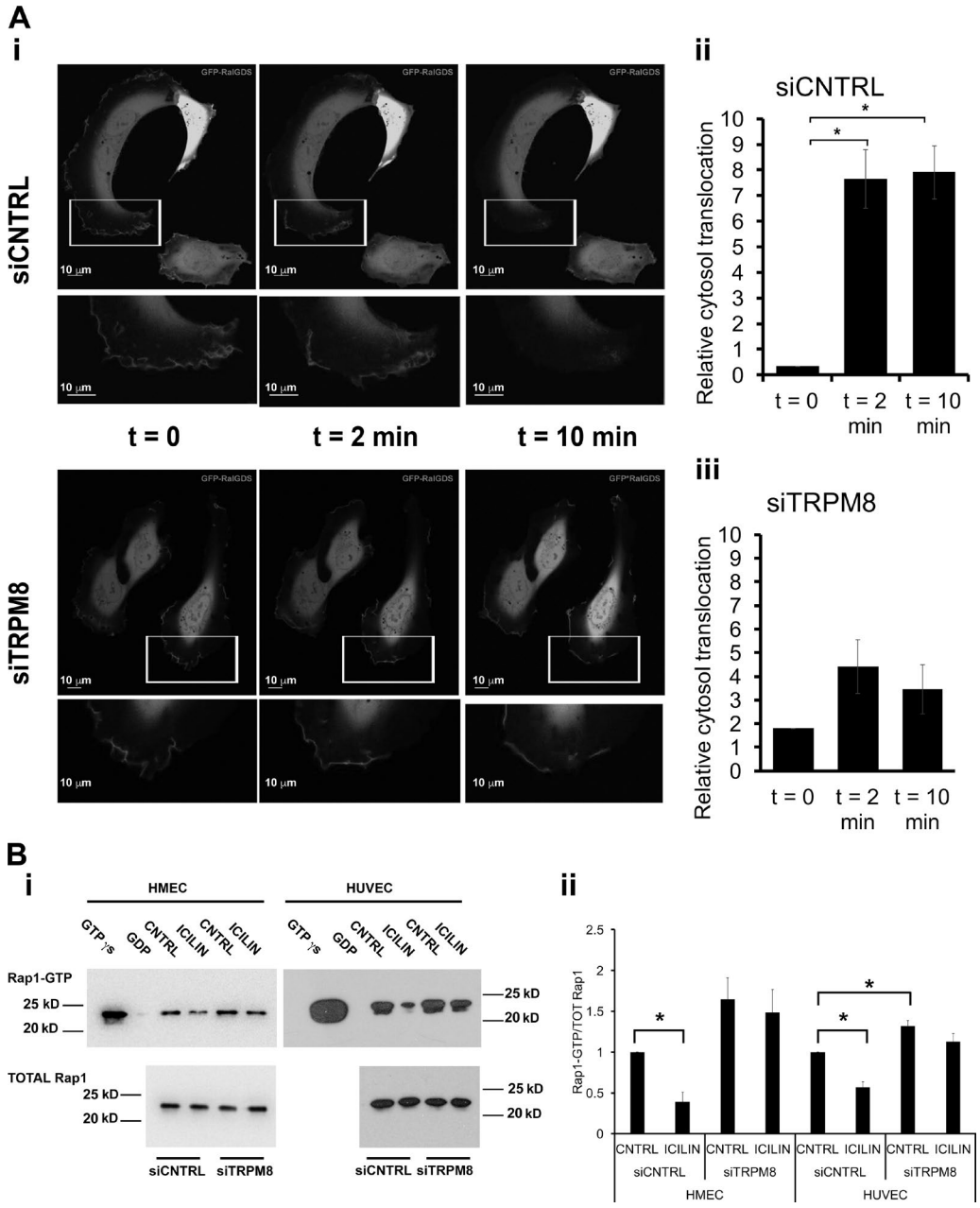

Figure 8. **Endogenous TRPM8 inhibits Rap1 activity.** (Ai) Live-cell imaging by confocal microscopy of ECs expressing GFP-RBD_{RalGDS} probe in control (siCNTRL) and siTRPM8-treated ECs (siTRPM8). Representative images showing RBD_{RalGDS} in siCNTRL- and siTRPM8-treated ECs at t = 0 and after 2 or 10 min of treatment with 10 μM icilin; the bottom parts of the figures represent enlargements of the inset (white lines) for each time point. (Aii and Aiii) Bar plot representing quantification of GFP-RBD membrane recruitment calculated as cytosol translocation as described in the method section. *, P < 0.05 (Wilcoxon–Mann-Whitney test). (Bi) Active Rap1 pull-down assay on HMEC or HUVEC silenced for TRPM8 (siTRPM8) or not (siCNTRL), in the presence or absence of icilin. (Bii) Quantification of the Rap1 activity normalized to HMEC siCNTRL or HUVEC siCNTRL condition. Data are expressed as mean ± SEM. *, P < 0.05 (Wilcoxon–Mann-Whitney test).

in the rescue of TRPM8-inhibited EC adhesion (Fig. 9 D). To verify this hypothesis, GTP-bound Rap1 pull-down assays were performed on ECs transfected with a Rap1-N17 overexpression plasmid. As shown in Fig. 9 C, the inhibitory effect of icilin on endogenous Rap1 was prevented when ECs were transfected with the inactive Rap1 mutant Rap1-N17. This would suggest a preferential interaction of TRPM8 cytosolic tails with the Rap1-GDP form.

To assess this hypothesis, we first studied the interaction of the TRPM8 GST-fused proteins with cell lysates overexpressing GFP-tagged Rap1-N17, and Rap1-V12. As for Rap1-WT, we detected a clear interaction between Rap1-N17 or Rap1-V12 with the TRPM8 N-terminal tail (GST-M8N) and to a lesser extent with the TRPM8 C-terminal tail (GST-M8C), whereas no interaction was observed with GST alone (Fig. 5 Ci). After quantification, Rap1-N17 showed a significantly stronger interaction for the TRPM8 N- and C-terminal tail as compared with Rap1-WT; moreover, only TRPM8 N-terminal tail interacted significantly more with Rap1-V12 (Fig. 5 Cii). We then assessed the possible direct association of Rap1 proteins with TRPM8

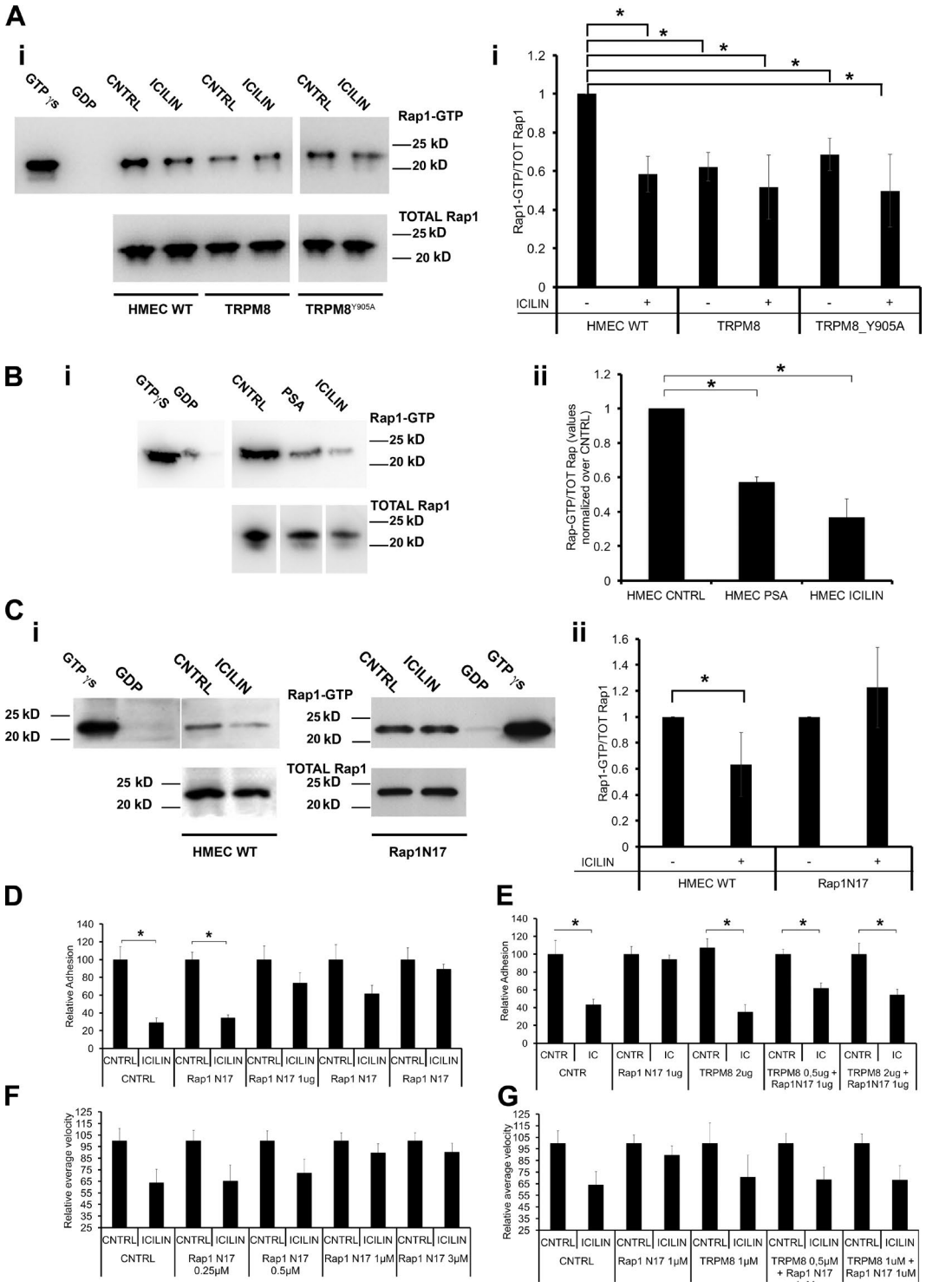

Figure 9. **TRPM8 activation promotes GDP-binding with Rap.** (A–C) Active Rap1 pull-down assay on HMECs transfected with 1 µg control vector (HMEC-WT; A), 1 µg TRPM8, 1 µg TRPM8^{Y905A}, or 1 µg Rap1-N17 (C) were treated or not with 10 µM icilin or 40 ng/ml PSA (B) for 10 min. Positive control: GTPγS; negative control: GDP. Lower bands refer to total Rap1. (Aii, Bii, and Cii) quantification of the Rap1 activity quantified as Rap1GTP over total Rap1 normalized to HMEC-WT condition (Aii) or untreated conditions (Bii and Cii). (D) Quantification of adherent EC to FN of HMECs transfected with 0.7, 1.0, 1.6, and 2.5 µg Rap1-N17 or control vector, treated or not with 10 µM icilin. *, $P < 0.05$. The data show adhesion in the icilin-treatment group normalized to control conditions. (E) Quantification of adhesion to FN of HMECs transfected with 1 µg Rap1-N17 and/or 0.5 or 2 µg TRPM8, treated or not with 10 µM icilin. *, $P < 0.05$. The data show adhesion in the icilin-treatment group normalized to control conditions. (F and G) Quantification of the mean relative velocity of a virtual cell expressing basal 0.2 µM TRPM8, treated or not with icilin, after the addition of different amounts of Rap1-N17 and/or of exogenous TRPM8. The values shown are means of 100 simulations. Error bars show standard deviations. The data show velocity in the icilin-treatment group normalized to control conditions.

C termini, by translating Rap1-WT, Rap1-N17, and Rap1-V12 in vitro with FluoroTect (Fig. 5 D). The subsequent GST pull-down assay revealed that only the inactive Rap1-N17 mutant interacted with TRPM8 (Fig. 5 D). This result was further validated by repeating the GST pull-down assay, but this time using only the Rap1-WT loaded with an excess of 1 mM GDP or 100 µM GTP. In line with the results obtained using the Rap1 mutants, GDP-loaded Rap1-WT interacted with the N terminus of the TRPM8 channel, whereas no interaction was detected when overloading with GTP or with unloaded Rap (Fig. 5 E). Collectively, the GDP-bound Rap1 (Fig. 5 E) as well as the GST-fused TRPM8 termini pull-down assays (Fig. 5 D) confirm the hypothesis for a selective interaction affinity of TRPM8 for Rap1-GDP. To strengthen the idea of a GTPase inhibitor–like effect of TRPM8 in sequestering inactive Rap1-N17, we performed a new set of time-lapse confocal experiments. We performed a double transfection of GFP-Rap1-WT or GFP-Rap1-N17 together with ER-DsRed in ECs. Although GFP-Rap1-WT was localized at the PM, at the leading edge of migrating ECs (Fig. 10 A), GFP-Rap1-N17 was already localized intracellularly (Fig. 10 B) instead of being internalized upon TRPM8 activation by icilin. This effect was quantified by measuring the distance between GFP-Rap1-WT or GFP-Rap1-N17 and ER-DsRed, as well as between GFP-Rap1-WT or GFP-Rap1-N17 fluorescent signals and the cell border, as previously described (see Fig. 6 and 7). The GFP-Rap1-WT/ER-DsRed distance significantly diminished starting 2 min after icilin treatment. Concomitantly, the distance between GFP-Rap1-WT and the cell membrane increased, suggesting that GFP-Rap1-WT was effectively internalized (Fig. 10 Ci). However, when cells were transfected with GFP-Rap1-N17, no significant difference in the GFP-Rap1-N17/ER-DsRed or the GFP-Rap1-N17/PM distance was observed after icilin treatment (n = 6/7 cells, four independent experiments; Fig. 10 Cii).

These data indicate how TRPM8 could exert an inhibitory effect on Rap1 activity by sequestering Rap1-GDP in intracellular compartments, likely the ER, thus inhibiting its localization to and activation at the PM and consequently impairing the β1-integrin–dependent adhesion of ECs to and migration on FN.

Discussion

TRPM8 functional expression has been recently suggested in ECs (Johnson et al., 2009; Mergler et al., 2013; Sun et al., 2014). Our data support TRPM8 expression in ECs by showing not only TRPM8 protein expression in different ECs but also its dramatic down-regulation in different clones of tumor-derived ECs. We further show that the EC TRPM8 shows an intracellular distribution and exerts an inhibitory effect on integrin-dependent cell-to-ECM adhesion, migration, endothelial tube formation, and in vitro sprouting. We therefore propose here a novel molecular mechanism by which TRPM8 interacts with the small GTPase Rap1 preferentially in its GDP-bound state, inhibiting its function and consequently impairing the activation of a major inside-out signaling pathway that is known to activate integrin and thus mediate cell adhesion and migration. The TRPM8 inhibitory role on cell migration is in accordance with previous data; it has recently been proposed that TRPM8 could have a protective function in metastatic prostate cancer by impairing the motility of these cancer cells (Gkika et al., 2010, 2015).

We show that ECs express TRPM8 intracellularly, localized close to the ER (Fig. 1). The intracellular localization of TRPM8 has been previously observed, although its role has not been fully elucidated (Zhang and Barritt, 2006; Bidaux et al., 2007; Wondergem et al., 2008). As shown by standard experiments silencing endogenous TRPM8 or overexpressing exogenous TRPM8 (Figs. 2, 3, and 5), we unveil how intracellular TRPM8 in ECs mimics the functional effects of classic surface TRPM8 on cell adhesion and migration. Our data are also supported by a modeling approach showing that cell adhesion and migration are strictly dependent on basal TRPM8 activity and on its expression levels rather than its localization (Fig. S3). Importantly, we show that the expression and constitutive activity of TRPM8 are sufficient to exert its functional effects, inhibiting EC–ECM adhesion and EC migration.

One of the more interesting novel findings of this paper is the pore-independent function of TRPM8 on both EC migration and Rap1 inhibition; indeed, using an engineered pore mutant TRPM8 channel, we still observed an inhibition of migration and Rap1 activity similar to that of wild-type TRPM8 (Figs. 2 and 9). In contrast, we clearly show that the inhibitory effect on migration was activated by icilin or menthol, well known TRPM8 gating activators (Baez et al., 2014; Bidaux et al., 2015). These data are surprising and raise questions about the possible effects of icilin and menthol on TRPM8 besides pore gating. Although a crystal structure of TRPM8 has not been reported yet, the structure of TRPV1 has recently been resolved in distinct conformations (Cao et al., 2013). Interestingly the authors showed that in the presence of toxins and capsaicin (which binds S1–S4 modules similarly to menthol for TRPM8) beside the movement in the outer pore and rearrangements in the lower gate, movement of the S4–S5 linker and S6 is also accompanied by lateral displacement of the TRP domain, which is in turn suggested as a point of structural integration that facilitates allosteric coupling between channel domains (Liao et al., 2013). These data could support the hypothesis that icilin and menthol promote conformational changes that are reflected in other functions of the channel besides gating.

Similar non-conductive roles for channel proteins have been described previously, and in particular, modulation of intracellular pathways has been reconducted to enzymatic roles of channel proteins or conformational coupling with other proteins, ultimately converging onto the transcriptional regulation of cancer-related genes. In contrast, there is mounting evidence for non-conductive roles for TRP channels proteins as regulators of cytoskeletal dynamics (Vrenken et al., 2015). As an example, TRPP1, also known as PKD1, displays a clear channel-independent role in the regulation of focal adhesion turnover by interacting with FAK and paxillin (Joly et al., 2006).

We show that the effect of TRPM8 is mediated by an inhibition of the inside-out signaling pathway that drives the activation of the β1-integrins as also supported by the inhibition of TRPM8-mediated decrease in cell adhesion by means of the specific rat monoclonal antibody 9EG7, which recognizes a cryptic epitope that is exposed only in the EGF2 domain of conformationally active β1-integrins (Fig. 4 A), and the dramatic inhibition of β1-integrin activation, as detected by 9EG7 (Fig. 4 C), in agreement with the important role played by β1-integrins in the control of EC adhesion and migration (Serini et al., 2006; Bussolino et al., 2009). Moreover, ion channels, including TRP channels, are known to modulate cell migration by directly or indirectly impinging on integrin-linked pathways

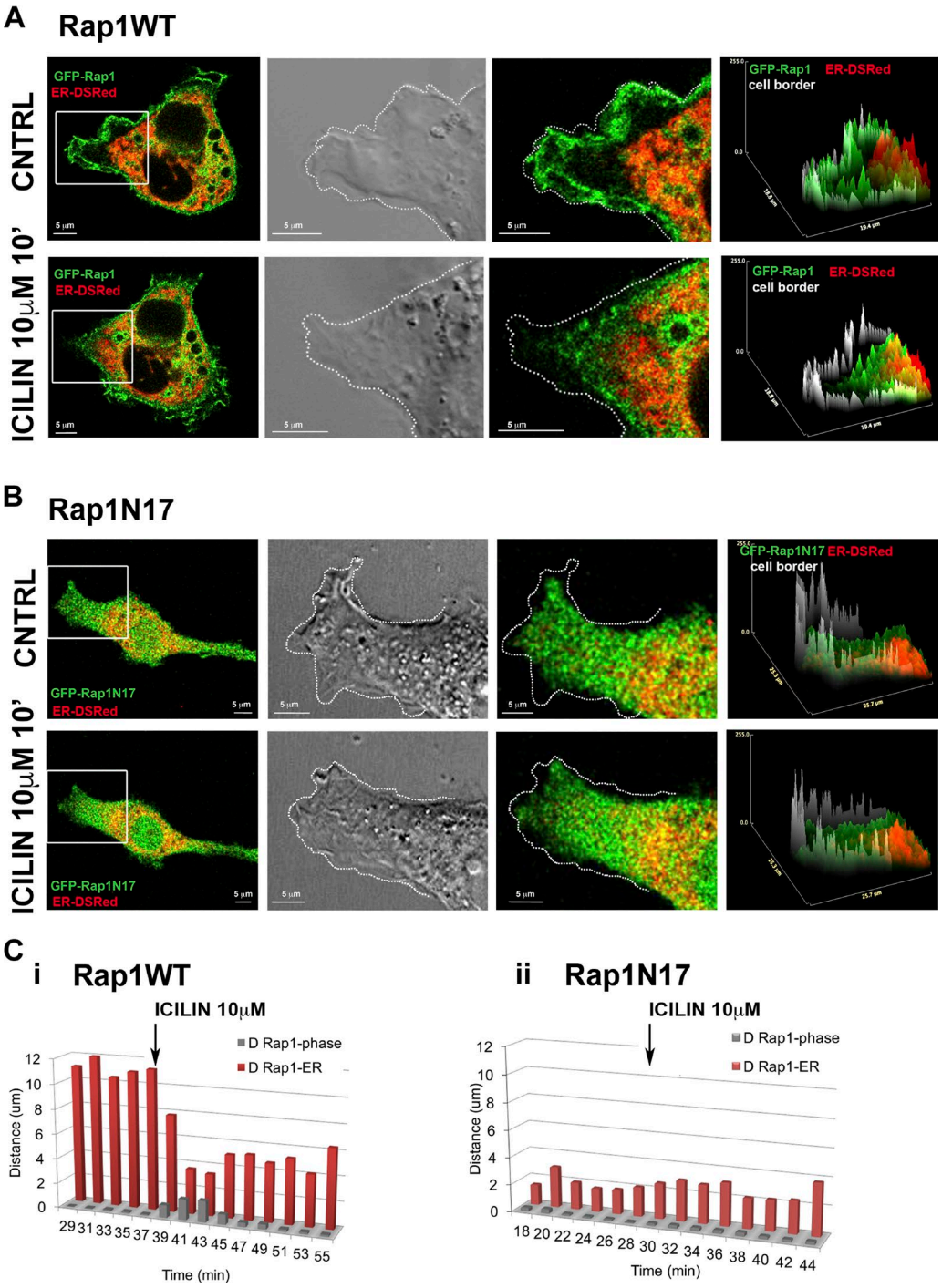

Figure 10. **TRPM8 activation promotes internalization of Rap1 WT, but not Rap1-GDP.** Live-cell imaging of ECs performed using confocal microscopy. Representatives pictures of ECs cotransfected with ER-DsRed and Rap1-WT-GFP 1 µg (Rap1WT; A) or Rap1-N17-GFP 1 µg (Rap1N17; B) at t = 0 and after 10 min of treatment with 10 µM icilin. Rap1 is labeled in green, ER is labeled in red, and PM is marked in gray. In the surface plot (on the right), it is possible to appreciate the colocalization of Rap1 and ER. We chose to label the ER for experimental simplicity, as we have previously demonstrated (Fig. 5) that TRPM8 is closely related to the ER in terms of localization and dynamics. (C) Histograms showing the means of the distances measured in plot profile between Rap1 and ER (red) and between Rap1 and the PM (gray) in ECs transfected with Rap1-WT and Rap1-N17.

(Pillozzi et al., 2007; Thodeti et al., 2009; Jacquemet et al., 2016). Our findings on TRMP8 are in agreement with previous observations concerning other endogenous inhibitory signals, such as those elicited by semaphorins (Serini et al., 2003), that exert an essential permissive role in the execution of this complex morphogenetic process, such as vascular morphogenesis, by inhibiting integrin-mediated adhesion of ECs to the ECM, allowing the de-adhesion necessary for vascular remodeling.

A major discovery of our study is the identification of the intracellular mechanism involved in TRPM8 function. Several studies have revealed that TRPM8-mediated intracellular functions are regulated by partner proteins. In particular, we have

recently described a whole list of intracellular proteins that interact with TRPM8, and we showed that the novel family of TCAF proteins mediates its inhibition of cell migration in prostate cancer cells (Gkika et al., 2015). Here, we focused on another TRPM8-partner protein that is part of the recently published list (Gkika et al., 2015) and revealed a novel Rap1-dependent molecular mechanism by which TRPM8 inhibits β1-integrin function in ECs (Fig. 4). Rap1 is indeed a key player in the signaling pathways that drive integrin activation in several cell types, including ECs (Bos, 2005; Boettner and Van Aelst, 2009). Here, we provide compelling evidence that its interaction with TRMP8 affects Rap1 function and localization. In this regard, it has previously been reported that the steady-state distribution of Rap1 depends on its guanine nucleotide–binding state; in particular, GTP-bound Rap1 is up-regulated at the PM in conjunction with its activation, whereas the nucleotide-free form of Rap1 is observed on cytoplasmic vesicles, but not at the PM (Bivona et al., 2004).

Upon the further stimulation of TRPM8 by icilin, we observed the intracellular retention of Rap1, which is therefore no longer able to shuttle from the ER to the PM; this retention is consistent with its close intracellular localization with both TRPM8 and the ER (Figs. 6 and 7). Moreover, the intracellular retention of Rap1 by TRPM8 inhibits Rap1-GTP loading and activation both in live cells as well as in vitro (Figs. 8 and 9). We therefore propose a model in which TRPM8 exerts an inhibitory effect on Rap1-GTP loading and functional activation by sequestering the GDP-bound inactive form of Rap1, thus decreasing the amount of Rap1 that is available for cycling from the inactive to the active form (GTP-bound and on the cell surface). This function of TRPM8 ultimately results in the inhibition of integrin activity, thus leading to the inhibition of EC adhesion and migration. This hypothesis is supported by different evidences: first, the direct interaction between Rap1 and TRPM8 N- and C-terminal tails is clearly detectable in the presence of GDP-loaded Rap1-WT or inactive GDP-bound Rap1-N17 mutant, but not with unloaded or GTP-loaded Rap1-WT (Fig. 5). Second, Rap1 activity is strongly increased by TRPM8 down-regulation (Fig. 8). Finally, the saturation of TRPM8-Rap interaction sites in cells overexpressing the inactive GDP-bound Rap1-N17 mutant on Rap1 activity as well as on cell adhesion, which can in turn be reversed by overexpressing TRPM8 in ECs (Fig. 9). Indeed, the excess of Rap1-N17 mutant in these cells binds to and eventually saturates TRPM8, thus allowing endogenous Rap1 to be cycled to Rap1-GTP and resulting in β1-integrin activation and EC adhesion and migration.

It is known that TRPM8 channels, like most TRP channels, are modulated by G proteins, as is the case for the Gi-coupled α2A-adrenoreceptor, which inhibits TRPM8 activity (Bavencoffe et al., 2010). A direct interaction between TRPM8 and G proteins has recently been described. Zhang et al. (2012) have demonstrated that the G protein Gαq directly binds to and inhibits TRPM8; moreover Gαq binds to TRPM8 even when inactive, and this binding is not enhanced by the activation of Gαq, supporting our hypothesis of TRPM8-Rap1–inactive binding. Conversely, another recent study has reported an interaction between TRPM8 and Gαq, showing that the activation of TRPM8 causes the downstream activation of the metabotropic glutamate receptor–Gαq-PLC pathway (Klasen et al., 2012). This study supports our data and raises the possibility not only that G proteins influence the gating of TRPM8, as previously shown, but also that TRPM8 gating may also influence G proteins and small G proteins such as Rap1, as we have shown here. In contrast, the interaction between Rap1 and the transmembrane proteins has recently been shown; semaphorin-mediated plexin dimerization locally inhibits Rap activity. In particular, these findings connect transmembrane protein signaling to Rap-mediated signaling, showing how small GTPases are used for spatial and temporal control of cell behavior (Wang et al., 2012). Our data suggest that TRPM8 could act similarly to a GDI-like protein, sequestering and inhibiting Rap1. Interestingly, in contrast to the classic GTP/GDP switch that regulates GTPase activity, an alternative nonconventional GDI mechanism mediated by the 14-3-3 proteins has recently been described to inhibit Rap1 and other small GTPase proteins, facilitating their extraction from their site of action in membranes and keeping them inactive by sequestration in the cytoplasm (Riou et al., 2013). Moreover, Lilja et al. (2017) recently reported an unexpected Ras-binding domain in SHANK3 protein that acts as an integrin activation inhibitor by sequestering active Rap1 and R-Ras via the SPN domain and thus limiting their bioavailability at the PM. Along these lines, our work uncovers a new role for the TRPM8 channel in ECs, where it acts as a transmembrane Rap1 inhibitor that, by sequestering Rap1 at the ER, hinders its activation and its translocation to the cell surface, ultimately impairing β1-integrin activation, cell adhesion, migration, and spheroid sprouting.

Although the present paper is mainly focused on vascular EC, TRPM8–Rap1 interaction and function is not confined to this particular type of cells but is crucial and generalized. In particular, we showed that TRPM8-Rap1 native interactions are clearly detected in a prostate cancer sample (as presented in the interactome protein list reported by Gkika et al., 2015), where TRPM8 plays a similar role in cell migration as in ECs; in contrast, we confirmed GST pull-down in an overexpression system of HEK cells.

The identity of the endogenous TRPM8 activator still needs to be fully identified. However, we provide evidence that PSA inhibits migration of ECs and significantly reduces the amount of active Rap1-GTP bound similarly to icilin treatment. These data are in agreement with the role for PSA in prostate cancer cell migration via TRPM8 activation previously described by us (Gkika et al., 2010). In particular we suggested that the activity of PSA on TRPM8 channels was not direct but mediated by bradykinin 2 receptor (Gkika et al., 2010) and therefore can act also on the ER form of the channel, which is the one present in ECs. Moreover, the antiangiogenic role of PSA has been reported by several groups in vitro and in vivo and is not dependent on its proteolytic activity (Fortier et al., 2003; Chadha et al., 2015). Collectively, our results reveal a new role for TRPM8 as a Rap1 inhibitor that arrests EC migration, whereas this effect could be regulated by PSA, an endogenous activator of the channel in vivo.

Materials and methods

Cell culture

We used BTECs, HMECs, HUVECs, HUAECs, and HEK-293 cells with inducible TRPM8 expression (HEK-TRPM8).

BTECs were obtained from human breast lobular-infiltrating carcinomas and were isolated with an anti-CD105 antibody coupled to magnetic beads by magnetic cell sorting using the MACS system (Miltenyi Biotec) as previously described (Bussolati et al., 2003; Grange et al., 2006). BTECs were isolated and extensively characterized by B. Bussolati (Grange et al., 2006). In particular, cell preparations of BTECs were obtained from four different tumors. All BTECs

were characterized for EC marker expression. To dispel the possibility that contaminating tumor cells may influence our results, the B-TEC01 cell line was cloned by limited dilution and obtained and characterized six different clones. All these clones confirmed the same pattern of endothelial marker expression as the progenitor B-TEC01 cell line. One of those clones was used in the present paper.

HMECs were obtained from the derma using an anti-CD31 antibody and MACS. HMECs from the derma were immortalized by the infection of primary cultures with a replication-defective adeno-5/SV40 virus as previously described (Cassoni et al., 2006; Fonsato et al., 2008). Both BTECs and HMECs were grown in complete EndoGRO-MV-VEGF (EMD Millipore) supplemented with 50 µg/ml gentamicin (Cambrex). Cells were used at passages 3 to 15. BTECs were cultured on a coating of 1% gelatin. Periodically, cells were characterized by their morphology and expression of a panel of endothelial antigens such as CD105, CD31, Muc-18 (CD146), CD44, and VEGF receptor 2.

HUVECs and HUAECs were isolated from the umbilical cord (from G. Serini's laboratory; see Sandri et al., 2012) and growth in M199 medium completed with cow brain extract, heparin sodium salt from porcine intestinal mucosa (0.025 mg/500 ml), penicillin/streptomycin solution, and 20% FBS (Sigma-Aldrich). HEK-293 and HEK-TRPM8 cells were grown in DMEM (Invitrogen) supplemented with 10% FCS (Poly-Labo; Seromed), 5 mM L-glutamine (Sigma-Aldrich), and 100 mg/ml kanamycin (Sigma-Aldrich). Cell were cultured as described in (Thebault et al., 2005b).

Gene silencing and overexpression

Gene overexpression in HMECs, BTECs, and HEK cells was obtained by nucleofecting 0.5–1.0 × 10^6 cells with the electroporator Amaxa Nucleofector II (Lonza) and Nucleofector Kits for Primary Endothelial Cells or Nucleofector KitV (Lonza) according to the manufacturer's instructions, using the program M-003 for ECs or A-023 for HEK cells.

For siRNA-mediated silencing, the day before oligofection, HUVECs or HMECs were plated in six-well dishes at a concentration of 12 × 10^4 cells per well. Oligofection (Oligofectamine; Life Science) of siRNA duplexes was performed according to manufacturer's protocols. In brief, ECs were transfected twice (at 0 and 24 h) with 200 pmol siLuc (control) or siTRPM8, and 72 h after the second oligofection, HUVECs were lysed or tested in functional assays.

The siTRPM8 sequence (5′-UAUCCGUCGGUCAUC UA(dTdT)-3′) is located at position 236 on the TRPM8 mRNA (GenBank accession no. AY328400). For control silencing, siRNA against Luciferase (siLuc; Eurogentec) was used.

The constructs used for this work were plasmids carrying the sequences of hTRPM8pcDNA4 (plasmid wild-type, Y905A, E906A; 2 µg for transfection) already available in our laboratory, as previously described (Thebault et al., 2005a; Bidaux et al., 2015); GFP-Rap1-WT or human influenza agglutinin (HA)–tagged (1 µg for transfection; from G. Serini); GFP-Rap1-N17 (0.25–2.5 µg for transfection; from G. Serini); GFP-Rap1-V12 or HA-tagged (0.7–1.6 µg for transfection; from G. Serini), ER-DsRED (DsRed2 fused to the ER targeting sequence of calreticulin; 1 µg; from Takara Bio Inc.) as indicated in the text and figures, and pEGFP-RalGDS-RBD (from M.R. Philips, as previously characterized; Bivona et al., 2004).

Western blot analysis

Cells were seeded in Petri dishes with the appropriate medium and grown to a confluency of 80%. Before cell lysis, Petri dishes were kept on ice and washed in ice-cold PBS twice. Cells were lysate in the presence of RIPA buffer (25 mM Tris-HCl, pH 7.6, 150 mM NaCl, 1% NP-40, 1% sodium deoxycholate, and 0.1% SDS) containing the following protease inhibitors: 2 mg/ml aprotinin, 1 mM Na orthovanadate, 0.1 mM PMSF, and 10 mM NaF. Lysates were centrifuged at 4°C for 15 min at 10,000 *g*. Protein concentrations were determined using a bicinchoninic acid kit (Sigma-Aldrich) following the manufacturer's instructions. Conditions for SDS-PAGE and Western blotting were assessed as previously described (Fiorio Pla et al., 2012b). Polyvinylidene fluoride membranes were properly blocked and then incubated overnight with rabbit anti–TRPM8 (1:400 Alomone) or rabbit anti–TRPM8 (1:400; ab109308; Abcam), anti–Rap1 (1:1,000; Thermo Fisher Scientific), anti–Fak or anti–phospho-Fak (Ty397; 1:200; Santa Cruz Biotechnology, Inc.), and anti–β-actin (Sigma-Aldrich) antibodies. The membrane was then washed with TBS containing 0.1% Tween 20 and incubated with the appropriate horseradish peroxidase–conjugated antibodies (Santa Cruz Biotechnology, Inc.). Chemiluminescence assays were conducted using the SuperSignal West Pico chemiluminescent substrate (Thermo Fisher Scientific). To quantify differences in protein expression, the ratio between TRPM8 and actin expression or between phospho-Fak and Fak expression (each normalized to actin) was evaluated.

Immunoprecipitation assay

Cells were cotransfected with a his-tagged hTRPM8pcDNA4 plasmid (wild-type, Y905A, E906A), HA-tagged rap1. 48 h after transfection, cells were washed twice with PBS and incubated for 60 min on ice in lysis buffer (1% Triton X-100, 1% sodium deoxycholate, 150 mM NaCl, 10 mM $NaKPO_4$, pH 7.2, and antiprotease cocktail; Sigma-Aldrich). After centrifugation (12,000 *g* for 10 min at 4°C) of the lysates, protein concentration was determined by the BCA assay (Thermo Fisher Scientific), and equal amount of supernatants were incubated overnight at 4°C with 2 µg of a mouse anti–HA antibody (H3663; Sigma-Aldrich) immobilized on protein A/G PLUS agarose beads (Santa Cruz Biotechnology, Inc.) in IP buffer (20 mM NaH_2PO_4 and 150 mM NaCl, pH 8). The pellet was washed three times in IP buffer, resuspended in SDS sample buffer, heated at 37°C for 30 min, separated on 4–20% precast SDS-PAGE gels (Bio-Rad), and analyzed by immunoblotting using rabbit anti–HA (1:2,000; ab9110; Abcam) and rabbit anti–TRPM8 (1:400; ab109308; Abcam) antibodies.

Each experiment was repeated at least three times.

Biotinylation assay

The biotinylation assay was performed after homogenizing cells in 1 ml lysis buffer as described previously (Gkika et al., 2010) using the NHS-LC-LC-biotin kit (Thermo Fisher Scientific). Biotinylated proteins were precipitated using neutravidin-agarose beads (Thermo Fisher Scientific). TRPM8 expression was analyzed by immunoblotting of the precipitates (PM fraction) or of total cell lysates using anti-TRPM8 antibody (Alomone).

PLA

Duolink in situ red starter kit goat/rabbit (Sigma-Aldrich) was used for this experiment. HMECs transfected or not with siTRPM8 were seeded at 20 × 10^3 cells per confocal FluoroDish (World Precision Instruments). Cells were fixed and permeabilized with 4% platelet activating factor for 10 min. After permeabilization, cells were incubated in the blocking buffer (provided with the kit) for 30 min at 37°C in a humidified chamber. Cells were incubated with the primary antibodies diluted in the antibody diluents for 2 h at room temperature (goat anti–TRPM8 antibody, ABIN572229, 1:200; Antibodies-online; rabbit anti-Rap1, MA5-15052, 1:200; Thermo Fischer Scientific). For the rest of the protocol, the manufacturer's instructions were followed. Recordings were performed by confocal imaging (LSM700; ZEISS) using z-stack superposition (Zen 2010 software; ZEISS). Appropriate

controls were performed by incubating with both primary antibodies separately (Fig. S5 G).

RNA isolation and real-time PCR

Total RNA was isolated using TRIzol Reagent (Thermo Fisher Scientific) according to the manufacturer's protocol and quantified spectrophotometrically (Nanodrop ND-1000). For gene expression analysis, quantitative real-time PCR was performed. In brief, first-strand cDNA was produced from 200 ng total RNA using the High Capacity cDNA Reverse Transcription kit (Applied Biosystems).

Quantitative real-time PCR experiments were performed in 20-µl reaction mixture containing 5 ng cDNA template, the sequence-specific oligonucleotide primers (purchased from MWG-Biotech, Eurofins Genomics) and the Power SYBR Green PCR Master Mix (Applied Biosystems). 18s was used to normalize RNA inputs. The following TRPM8 sequence-specific oligonucleotide primers were used: forward, 5′-ACA CCCAACCTGGTCATCTCA-3′; reverse, 5′-TGCCCCTTTAGACTG AGCGA-3′; 18S ribosomal RNA: forward, 5′-CAGCTTCCGGGA AACCAAAGTC-3′; reverse, 5′-AATTAAGCCGCAGGCTCCACTC-3′. The comparative Ct method was adopted for relative quantification of gene expression and 18s was used to normalize RNA inputs. Fold-change expression respect to HMECs was calculated for all samples.

Migration assay

Cell motility was investigated by the migration of cells into a scratch "wound" made on a confluent monolayer as previously described (Pupo et al., 2011). Cells were grown to confluency in 24-well culture plates coated with 1% gelatin. Cell monolayers were allowed to rest for 12 h in DMEM containing 2% FCS and a "wound" made by scraping the middle of the cell monolayer with a P10 pipette tip. Floating cells were removed by washing twice with PBS, and the cell monolayer was treated with test conditions (see Results). Cells did not undergo any significant degree of cell division during the experiments. Experiments were done using a Nikon Eclipse Ti-E microscope with a 4× objective. Cells were kept at 37°C and 5% CO_2 for all experiments; a photo was taken every 2 h using MetaMorph software. Cell migration into a wound was measured with MetaMorph software. Cell migration was assessed by measuring the distance between the two sides of the wound at each time point. Three separate wells were used for each condition; in each well, at least six fields were analyzed for each condition. At least three independent experiments were performed for each question asked. Obtained data were further analyzed using Excel to calculate the percentage of migration for each wound (difference of distances between cell fronts at two subsequent time points over distance at time = 0 h), and the percentage mean value for each condition was then calculated. Relative migration was calculated, evaluating the propagation of errors for the SEM. A nonparametric unpaired Wilcoxon–Mann-Whitney test was used to assess statistical significance.

In vitro vascular network formation

The in vitro formation of capillary-like structures was studied on growth factor–reduced Matrigel (BD) in 24-well plates. Cells (3.5×10^4 cells/well) were seeded onto a Matrigel coating in EndoGRO MV-VEGF complete medium and treatment conditions. Each experimental condition was performed in duplicate, and at least six fields for each well were analyzed for each independent experiment. At least three independent experiments were performed for each question asked. Cell organization on Matrigel was periodically observed with a Nikon Eclipse Ti E microscope using a Nikon Plan 10×/0.10 NA objective. Cells were kept at 37°C and 5% CO_2 during the experiment. Images were acquired at 2-h time intervals using MetaMorph software.

Image analysis was performed with ImageJ software. Images at 18 h of treatment were analyzed. The number of nodes (intersections formed by at least three detectable cells) and total tubule length (aligned cells connecting nodes) were measured for each field. The number of nodes and tubule length were normalized to maximum values and their sum for each condition was used to express the degree of organization into "capillary-like" structures in terms of arbitrary units. Graphs represent three independent experiments; error bars show SEM. A nonparametric unpaired Wilcoxon–Mann-Whitney test was used to assess statistical significance.

HUVEC sprouting assay

HUVEC collagen sprouting assay was performed as previously described (Korff et al., 2004). In brief, confluent monolayers of HUVECs were trypsinized and suspended in M199 complete culture medium plus 20% of M199 medium containing 2% methylcellulose (Methocel Stock medium) and seeded in nonadherent round bottom 96-well plates. Under these conditions, all suspended cells contribute to the formation of a single spheroid per well of defined size and cell number (800 cells per spheroid). Spheroids were cultured for 24 h and used for the corresponding experiments. HUVEC spheroids were suspended in Methocel Stock medium, enriched with 40% FCS, with or without different stimuli, and mixed with a volume of diluted collagen stock solution, previously prepared in ice (Korff et al., 2004). The spheroid containing collagen was rapidly transferred into a 48-well plate and allowed to polymerize (15 min) at 37°C after which 400 µl of M199 poor were added in each well. The plate was incubated at 37°C, 5% CO_2, and 100% humidity for 24 h. The following molecules were used for the stimulation of HUVEC spheroids: 10 ng/ml VEGF 165 (R&D Systems), 10 µM icilin, and 10 ng/ml VEGF 165 + 10 µM icilin.

HUVEC spheroids in 3D collagen matrix were fixed with 4% PFA for 10 min at room temperature and examined at 24 h after stimulation. Spheroids were imaged under bright field using the DMI 4000 B inverted microscope (Leica Biosystems). Analysis of the total area of sprouts per spheroid was performed on phase contrast images using the ImageJ software package applying a fix threshold and subsequently measuring the spheroid area.

Results are shown as mean ± SEM of four independent assays (total $n = 60$ spheroids per experimental condition), one of which is shown in the figure's panel. Results were analyzed by a two-tailed heteroscedastic Student's t test (*, $P \leq 0{,}05$; **, $P \leq 0{,}01$; and ***, $P \leq 0{,}001$).

Impedentiometric analysis

Impedentiometric analysis was performed to measure cell impedance with the RTCA DP Analyzer xCELLigence System (Roche). Cells were seeded onto a 1 µg/ml FN coating on a 16-well "E-Plate" that incorporates a sensor electrode array, allowing cells in the well to be monitored and assayed.

Adhesion assay

Cell adhesion was evaluated on 96-well plates using a coating of 1% gelatin or 0.25–2.0 µg/ml FN. Cells were detached using trypsin for 3 min, carefully counted and seeded at 3,000 cells per well in 100 µl growth medium (EndoGRO-MV-VEGF for HMECs and BTECs or complete M199 medium for HUVECs) under different conditions (see Results). It should be noted that the medium was not depleted for FN.

The 96-well plates were kept at 37°C and 5% CO_2 for 15 min and then washed twice with PBS. Cells were fixed in 4% PFA for 15 min and then washed twice with PBS. To stain cell nuclei, 1 µM DAPI was used for 15 min at 37°C.

Image acquisition was performed using a T-E microscope (Nikon) with a 4× objective and cell nuclei counted using the automatic cell count tool of ImageJ.

At least eight wells for each condition were analyzed in each independent experiment. At least three independent experiments were performed. A nonparametric unpaired Wilcoxon–Mann-Whitney test was used to assess statistical significance.

Haptotaxis assay

Haptotaxis assays were performed on 24-well plates containing ECs seeded onto 8-µm-pore membrane cell culture inserts (Corning), whose bottoms were coated with 1 µg/ml FN. After 24 h of the same growth medium (EndoGRO-MV-VEGF), 10 µM icilin was added to both the top and bottom chambers (to exclude chemotactic migration); control wells received no treatment. After 6 h, ECs on the underside of the insert were stained with Hoechst dye. Image acquisition was performed using a Nikon T-E microscope with a 4× objective, and cell nuclei were counted using the automatic cell count tool of ImageJ. Each experimental condition was performed in duplicate, and at least six fields for each well were analyzed for each independent experiment. At least three independent experiments were performed for each question asked. A nonparametric unpaired Wilcoxon–Mann-Whitney test was used to assess statistical significance.

Integrin activation immunofluorescence assay

80,000 HUVECs per slide were plated on 0.17-mm glass coverslips precoated with 3 µg/ml FN. The day after, the medium was replaced with 200 µl of an icilin treatment solution (10 µM icilin in M199 complete medium), and cells were treated for 15 or 30 min at 37°C. After the required time, the treatment was replaced with a solution containing the anti–β1-integrin antibody (10 µg/ml 9EG7 rat BD [1:50] in M199 complete medium), and cells were treated for 10 min at 37°C. Cells were washed once with 1× PBS and fixed with a solution PFA 2% in PBS for 10 min at room temperature. Cells were washed and permeabilized in 0.1% Triton 1× PBS for 2 min on ice and incubated with the appropriate Alexa Fluor–tagged secondary antibody (1:400 donkey anti–rat 488 and 1:10,000 DAPI Alexa Fluor; Thermo Fisher Scientific).

Cells were analyzed by using a TCS SPEII confocal laser-scanning microscope (Leica Biosystems) using LAS AF software (Leica Biosystems) for image acquisition. Acquisition was performed by adopting laser power, gain, and offset settings that allowed us to maintain pixel intensities (grayscale) within the 0 to 255 range and hence avoid saturation.

Analysis of confocal images was performed using the ImageJ software package measuring corrected total cell fluorescence as integrated density − (area of selected cell × mean fluorescence of background readings) (Burgess et al., 2010).

Results are the mean ± SEM of 15 cells per experimental condition, one of which is shown in the figure panels. Results were analyzed by a two-tailed heteroscedastic Student's *t* test (*, $P \leq 0.05$; **, $P \leq 0.01$; ***, $P \leq 0{,}001$).

Active Rap1 pull-down and detection assay

A pull-down and detection assay for active Rap1 was performed using the Active Rap1 Pull-Down and Detection kit from Thermo Fisher Scientific following the manufacturer's instructions.

The detection of GTP-bound Rap1 GTPase was obtained through specific protein interactions with the RalGDS protein–binding domain.

At least three independent experiments were performed for each question asked. A nonparametric unpaired Wilcoxon–Mann-Whitney test was used to assess statistical significance.

GST-fusion proteins and pull-down assay

TRPM8 N- and C-terminal tail GST-fusion proteins were produced and purified as described previously (Gkika et al., 2015). GST-fused purified proteins were then incubated with HEK cell lysates transfected with pEGFP-RAP-1, pEGFP-RAP-1N17, or pEGFP-RAP-1V12 plasmids (Bivona et al., 2004). For the direct interaction assay, the coding sequence of RAP-1-WT, RAP N17, and RAP V12 were subcloned in the pCMV TNT vectors (Promega) as EcoR1–Not1 fragments to produce them in vitro. Subsequently, Rap-WT and mutant proteins were translated in vitro using the TNT Quick Coupled Transcription/Translation Systems kit (Promega) and the FluoroTect GreenLys in vitro Translation Labeling System (Promega) as per the manufacturer's instructions. For GST pull-down experiments performed with Rap1-WT loaded with GDP and GTP, in vitro translated Rap1-WT was incubated with 10 mM EDTA followed by 1 mM GDP or 100 µM GTPγS for 30 min at 30°C with constant agitation. The sample was then placed on ice, 60 mM $MgCl_2$ was added, and the sample was vortexed.

Cell lysates or in vitro translated proteins were incubated overnight at 4°C together with the purified GST-fusion proteins. Subsequently, beads were washed extensively and bound proteins were eluted with SDS-PAGE loading buffer, separated on 4–20% wt/vol SDS-PAGE gels, and visualized by fluorescence imaging (Bio-Imager 600; GE Healthcare).

Calcium imaging

Cells were grown on glass gelatin-coated coverslips (gelatin coating was avoided for experiments using Tyrode physiological solution without Ca^{2+}) at a density of 5,000 cells/cm^2 for 24 to 48 h. 2 to 5 h before experiments, cells were starved in DMEM with 0% FCS. Cells were next loaded (45 min at 37°C) with 2 µM Fura-2 AM (Invitrogen) for ratiometric cytosolic Ca^{2+} ($[Ca^{2+}]i$) measurements as previously described (Fiorio Pla et al., 2010, 2012b). During the experiments, cells were continuously bathed with a microperfusion system.

Fluorescence measurements were performed using a Polychrome V spectrofluorometer (TILL Photonics) attached to a Nikon TE-2000-S (Nikon) microscope and Metafluor Imaging System (Molecular Devices) for image acquisition using 3-s intervals. During experiments, cells were maintained in a standard extracellular solution of the following composition: 145 mM NaCl, 5 mM KCl, 2 mM $CaCl_2$, 1 mM $MgCl_2$, 10 mM Hepes, and 10 mM glucose (NaOH to pH 7.35). Cells were continuously bathed with a microperfusion system. Each fluorescent trace (340/380 nm ratio) represents one ROI corresponding to cells in the chosen image field.

Peak amplitude (fluorescence intensity ratio, measured at 510 nm) was determined by the difference between the maximum and minimum values of fluorescence intensity before reaching the peak itself. For the estimation of peak amplitude, only responses that had a ΔEm340/380 >0.02 were considered.

Electrophysiology

BTEC or BTEC-TRPM8 expressing macroscopic membrane ion currents were recorded at 37°C or 22°C using the patch-clamp technique in its whole-cell configuration. The currents were acquired using a PC-9 amplifier (HEKA) and analyzed offline using Origin software (OriginLab Corporation). The extracellular solution (osmolarity 310 mosM/l) contained 150 mM NaCl, 5 mM KCl, 10 mM Hepes, 10 mM glucose, 1 mM $MgCl_2$, and 2 mM $CaCl_2$, pH 7.3 (adjusted with NaOH). The intracellular pipette solution (osmolarity 290 mosM/l) contained 140 mM CsCl, 10 mM Hepes, 8 mM EGTA, 1 mM $MgCl_2$, and 4 mM $CaCl_2$ (100 nM free Ca^{2+}), pH 7.2 (adjusted with CsOH). Patch pipettes were fabricated from borosilicate glass capillaries (World Precision Instruments). The resistance of the pipettes varied between 3 and 5 MΩ.

Necessary supplements were added directly to the respective solutions in concentrations that would not significantly change the osmolarity. Changes in the external solutions were performed using a multibarrel puffing micropipette with common outflow that was positioned in close proximity to the cell under investigation. During the experiment, the cell was continuously superfused with the solution via a puffing pipette to reduce possible artifacts related to the switch from static to moving solution and vice versa. Cells were kept at 37°C. TRPM8 activity activated by imposing 22°C to bath solution was recorded, followed by application of 10 µM icilin and 500 µM menthol, to maximally stimulate TRPM8 channel.

Confocal analysis

HMECs grown on glass coverslips were fixed using 4% paraformaldehyde and incubated with PBS containing 0.2% BSA, 0.1% Triton X-100, for 30 min at room temperature to block nonspecific binding and to permeabilize the cells. They were then incubated overnight at 4°C with PBS/5% nonimmunized serum containing a 1:200 dilution of the primary affinity-purified rabbit anti–TRPM8 polyclonal antibody (Alomone) and primary mouse anti–calnexin antibody. Cells were then washed with PBS and incubated with the secondary antibodies Alexa Fluor 546–labeled anti–rabbit IgG (dilution 1:2,000; Molecular Probes) or Alexa Fluor 488–labeled anti–mouse IgG (dilution 1:2,000; Molecular Probes) diluted in PBS for 1 h at room temperature. After rinsing three times in PBS, cells were incubated in the presence of DAPI to stain nuclei, the slides mounted with Mowiol, and the distribution of labeled proteins was analyzed using an LSM 780 confocal immunofluorescence microscope (ZEISS) equipped with an argon laser and 405-nm diode. Control experiments were performed without primary antibody.

For live-cell imaging experiments, HMECs were nucleofected with 1 µg TRPM8-YFP, 1 µg ER-DsRed, or 1 µg Rap1-GFP or double transfected with 1 µg ER-DsRED and 1 µg Rap1-GFP or 1 µg Rap1N17-GFP (as indicated in Results) or 0.5 1 µg GFP-RBD_{RalGDS}. For the experiments on TRPM8 down-regulation in HMECs, cells were first oligofected with siRNA against TRPM8 (siTRPM8) with a double pulse as described in Materials and methods. 48 h after the second pulse, HMECs were detached and nucleofected with 1 µg ER-DsRed and 1 µg Rap1-GFP or 0.5 1 µg GFP-RBD_{RalGDS}. 24h after this second transfection, cells were imaged using an LSM 780 confocal microscope equipped with an argon laser. Live cells were kept at 37°C and 5% CO_2 for all experiments, and confocal images were acquired every minute using the "perfect focus" option to maintain the same focal plane. After 1 h of acquisition, ECs were stimulated with 10 µM icilin or with a control solvent (DMSO 1:2,000 in PBS). Images were acquired using ZEN software and analyzed offline with ImageJ. For the analyses of GFP-RBD_{RalGDS}, we measured relative cytoplasmic translocation as previously described (Bivona and Philips, 2005). In brief for each cell, we drown at least two ROIs of identical size around a region of cytosol without membrane encroachment and around an area of distinct PM fluorescence for each cell analyzed. The fluorescence intensity (I) was determined for these ROIs at each time point (Fig. S2 C). Relative cytoplasmic translocation (R) was calculated as R = (Ics − Im)/Im, where Im and Ics are the fluorescence intensities of the regions of interest of membrane and cytosol, respectively. A nonparametric unpaired Wilcoxon–Mann-Whitney test was used to assess statistical significance. At least three independent experiments were performed for each experimental condition.

Mathematical model

The role of TRPM8 channels in controlling Rap1-dependent EC migration and adhesion was studied with a multiscale hybrid mathematical approach. In particular, at the lowest molecular level, a system of reaction-diffusion (RD) equations describes the spatiotemporal kinetics of the molecular variables of interest. A suitable version of the CPM, a mesoscopic spatial grid–based formalism (Glazier and Graner, 1993; Scianna and Preziosi, 2013), reproduced instead the dynamics of the cell as a whole, derived from an iterative minimization of the energy of cell deformation and stretching through stochastic fluctuations. These different submodels were then interfaced and integrated in a hybrid environment and directly impacted each other, with a constant interplay and flux of information between the different levels (see the next paragraph for an exhaustive description of the model). Variations in cell morphology were quantified by evaluating the relative area of a cell, given by the ratio $a_{cell}(t)/A_{cell}$, where $a_{cell}(t)$ is the actual area of the cell and A_{cell} is its initial area This value qualitatively also corresponded to the relative adhesion of cells under experimental conditions, especially in 2D computational settings (Scianna et al., 2013). Cell velocity was determined by the velocity of the cell center of mass, as described previously (Scianna et al., 2013). The mean values for cell velocity and relative area were evaluated over a timespan of 12 h.

Model hypothesis and considerations

The proposed multiscale hybrid theoretical approach is based on the following (minimal) set of assumptions, schematically represented in Fig. S2 B: (1) the mathematical model refers to the HMEC experimental model; (2) cell dynamics are modeled in 2D, using the quasi-3D approximation described previously (Marée et al., 2006); (3) the cell cytosolic region and the PM are explicitly reproduced, whereas the ER, because of its intricate reticular structure, is represented as a continuous network of varying density within the cytosol (Fink et al., 2000); (4) we model both the basal and the icilin-induced activity of TRPM8; (5) TRPM8 channels are distributed in the cytosolic region in accordance to the local density of the ER; (6) we keep track of the Rap1 that is active (R_a present both in the cytosol and in the membrane) or inactive (R_i, *l*ocalized only in the cytosol); (7) we introduce a further molecular variable, R_{am}, representing the complex Rap1-Riam-Talin-integrin-Fak localized in the PM; (8) Rap1 cycles between its active and inactive forms in the cytosol; (9) the membrane-bound Rap1-mediated assembly has a regulatory function of both cell adhesion and migration; and (10) TRPM8 inhibits Rap1 functions by sequestering the inactive RAP1-GDP-bound form. Such a sequestering activity is enhanced by ICILIN stimulation but is already active in TRPM8 at the basal state.

Such a collection of model hypothesis are consistent with the experimental observations presented throughout the paper. This allows us to provide coherent comparisons between in silico and in vitro outcomes and use the mathematical approach in a predictive manner, i.e., to determine the consequences in the cellular behavior of selected conditions, which would be hard to obtain by experimental setting manipulations. However, it is useful to remark that the theoretical approach does not incorporate each and every aspect and factor of the mechanisms involved in the problem of interest, as its derivation relies upon simplification procedures. In this respect, we can claim that the mathematical model deals with a "clean" cellular system and that its outcomes and predictions therefore have to be observed with a qualitative point of view.

Model description

The simulation domain is a 2D regular lattice $\Omega \in R^2$, formed by identical closed grid sites $x = (x,y)$. Each site is labeled by an integer number, $\sigma(x) \in N_+$, that can be interpreted as a degenerate spin originally coming from statistical physics (Ising, 1925; Potts, 1952). As classically adopted in CPMs, a neighboring site of x is denoted by x' and its overall neighborhood by Ω'_x (i.e., $\Omega'_x = \{x' \in \Omega : x' \text{ is a neighbor of } x\}$). Following the CPM extension proposed previously (Scianna

and Preziosi, 2012), the EC is represented as a compartmentalized element, composed of two subregions: a central cytosolic cluster and the surrounding PM. Each intracellular compartment consists of a set contiguous lattice sites sharing the same index $\sigma(x)$. In particular, the cytosol is defined as $\Sigma_{\sigma(x)=1} = \{x \in \Omega : \sigma(x) = 1\}$ and the PM as $\Sigma_{\sigma(x)=2} = \{x \in \Omega : \sigma(x) = 2\}$. The cell resides in a matrix-like substrate that is finally represented by an extended and isotropically distributed element $\Sigma_{\sigma(x)=0} = \{x \in \Omega : \sigma(x) = 0\}$ (Fig. S2 A). At each time *t,* the effective energy of the cell, whose minimization establishes its dynamics, is determined by a Hamiltonian functional: $H(t) = H_{adhesion}(t) + H_{shape}(t)$.

$H_{adhesion}$ is the general extension of Steinberg's differential adhesion hypothesis (Steinberg, 1970; Scianna and Preziosi, 2013), which is differentiated in the contributions from either the generalized contact tension between the cytoplasm and the PM or the effective adhesion between the cell and the matrix-like substrate: $H_{adhesion}(t) = \sum_{x,x' \in \Omega'_x} J_{\Sigma_{\sigma(x)=1},\, \Sigma_{\sigma(x')=2}} + \sum_{x,x' \in \Omega'_x} J_{\Sigma_{\sigma(x)=2},\, \Sigma_{\sigma(x')=0}}(t)$, where the coefficients $J's \in R$ are binding forces per unit area and are obviously symmetric with respect to their indices. In particular, we fix a high negative bond energy J_{Σ_1,Σ_2} to prevent the cell from fragmenting (Scianna and Preziosi, 2012; Scianna et al., 2013). The cell–substrate adhesiveness is instead assumed to be locally enhanced by the concentration of Rap1-mediated active integrin complexes in the PM, as $J_{\Sigma_{\sigma(x)=2},\, \Sigma_{\sigma(x')=0}}(t) = J_0 e^{-KR_{am}(x,t)}$, where $R_{am}(x,t)$ is the local amount of active integrin assemblies in the PM (compare Eq. 4). H_{shape} models the geometrical attribute of the cell, written as a nondimensional relative deformation in the following quadratic form (see Scianna and Preziosi, 2013 for a more detailed explanation):

$$H_{shape}(t) = \lambda_{el}(t)\left(\frac{a_{cell}(t) - A_{cell}}{a_{cell}(t)}\right)^2,$$

where $a_{cell}(t) = \Sigma x$: $\sigma(x) = \{1,2\}$ is the cell actual area and A_{cell} is its initial value. $\lambda_{el}(t) \in R_+$ is a mechanical modulus in units of energy relative to the cell deformability/elasticity; i.e., the ease with which the individual is able to remodel. Following experimental considerations suggesting a Rap1-mediated facilitation of cytoskeletal reorganizations, we set $\lambda_{el}(t) = \lambda_0 e^{-KR_{am}(cell,t)}$, where λ_0 is an intrinsic cell resistance to compression and $R_{am}(cell,t) = \sum_{x:\sigma(x)=\{1,2\}} R_{am}(x,t)$ evaluates the total amount of active integrin complexes within the cell (a similar relation is used in Scianna et al., 2011 for VEGF-activated vascular ECs during tubulogenic processes). The energy minimization algorithm consists of a modified Metropolis method for Monte Carlo–Boltzmann dynamics (Metropolis, 1953; Graner and Glazier, 1992; Glazier and Graner, 1993; Scianna and Preziosi, 2013). Procedurally, at each time step *t*, called Monte Carlo step (the basic unit of time of the model), a lattice site x_s (s for source) is selected at random and attempts to copy its spin, $\sigma(x_s)$, into one of its unlike neighbors, $x_t \in \Omega'_x : \sigma(x_t) \neq \sigma(x_s)$ (*t* for target), also randomly selected. In particular, if $\sigma(x_s)\,\sigma(x_s) = 2$ and $\sigma(x_t) = 0$, the cell is protruding, whereas if $\sigma(x_s) = 0$ and $\sigma(x_t) = 2$, the cell is retracting. Finally, if $\sigma(x_s) = 1$, the cell is reorganizing. Such a trial spin update is accepted with a Boltzmann-like probability function $P[\sigma(x_s) \to \sigma(x_t)]$, which takes into account also of the intercellular chemical state:

$$P[\sigma(x_s) \to \sigma(x_t)]\,(t) = \begin{cases} \tanh(\Psi R_{am}(x_s,t))\min\left\{1, e^{-\frac{\Delta H}{\Psi R_{am}(x_s,t)}}\right\} & \text{when cell is protruding;} \\ \min\{1, e^{-\Delta H}\} & \text{when cell is reorganizing;} \\ e^{-\Psi R_{am}(x_s,t)} & \text{when cell is retracting,} \end{cases} \quad (1)$$

where ΔH is the net difference of the system energy caused by the proposed change of domain configuration, R_{am} is, as seen, the local amount of active integrin complexes and ψ is a proper constant. In particular, in Eq. 1, we model the experimentally provided Rap1 influence in filopodia extensions and membrane ruffles.

The inactive form of Rap1 satisfies an RD equation of the form:

$$\frac{\partial R_i}{\partial t} = D_R \Delta R_i + k_{off_R} R_a - k_{on_R} R_i - \Gamma R_i \rho \text{ in } \Sigma_1 \quad (2)$$

where D_R represents the constant cytosolic diffusion of Rap1 and k_{on_R} and k_{off_R} its kinetics rate of activation and inactivation, respectively. The last term at the right-hand side of the equation describes instead the GDI-like effect of TRPM8 in sequestering the inactive form of Rap1: in particular, $\rho(x) = e^{-d(x,x_{CM})}$, where x_{CM} is the cell center of mass, measures a normalized local density of the ER, which, as reported from electron microscopy, increases in perinucear regions (Fink et al., 2000). Finally, Γ is a constitutive law that measures the sequestering rate of inactive Rap1 performed by TRPM8. In particular, Γ varies with the different experimental conditions as follows:

$$\Gamma = \begin{cases} k_{on_T} T & \text{NO ICILIN;} \\ k_{on_{T_i}} T & \text{ICILIN;} \\ k_{on_T} T\left(1 - \frac{k_{on_T}}{1 + k_{on_T}} \frac{R_{n17}}{1 + R_{n17}}\right) & \text{NO ICILIN and Rap1-N17;} \\ k_{on_{T_i}} T\left(1 - \frac{k_{on_{T_i}}}{1 + k_{on_{T_i}}} \frac{R_{n17}}{1 + R_{n17}}\right) & \text{ICILIN and Rap1-N17.} \end{cases} \quad (3)$$

In Eq. 3, T measures the homogeneous and constant-in-time local amount of TRPM8, which is given by the sum of endogenous and exogenous (added by transfection) channels, i.e., $T = T_{er} + T_{ex}$. k_{on_T} and $k_{on_{T_i}}$ are the rate of sequestering of inactive Rap1 characterizing, respectively, TRPM8 with a basal activity and icilin-activated TRPM8: in this respect, it is consistent to assume $k_{on_T} < k_{on_{T_i}}$ (we are further assuming that ICILIN stimulation analogously enhances the activity of all channels). Finally, R_{n17} model the concentration of exogenous Rap1-N17 (experimentally obtained by the corresponding transfection), which is assumed, for the sake of simplicity, to be homogenous in the whole cell cytosol.

The dynamics of the active form of Rap1 are instead described by:

$$\frac{\partial R_a}{\partial t} = D_R \Delta R_a - k_{off_R} R_a + k_{on_R} R_i + k_{off_M} R_{am} - k_{on_M} R_a \text{ in } \Sigma_1 \cup \Sigma_2,$$

where k_{on_M} and k_{off_M} represent the rate of assembly and disassembly of the membrane-bound integrin complexes (the other parameters have been already introduced in Eq. 2). Finally, the local amount of Rap1-mediated integrin complexes is determined as

$$\frac{\partial R_{am}}{\partial t} = D_{R_{am}} \Delta R_{am} - k_{off_M} R_{am} + k_{on_M} R_a \text{ in } \Sigma_2, \quad (4)$$

where $D_{R_{am}}$ is a constant diffusion rate along the membrane.

Model parameter setting

The characteristic length of each lattice site is 1 µm. The lattice of the CPM and the discretized PDEs use the same resolution. One Monte Carlo time step corresponds to 0.1 s, and the same time step is used to numerically integrate the PDEs. Diffusion processes are integrated using an explicit Euler method, with sufficiently small time-steps to guarantee numerical stability and with no flux boundary conditions. A summary of the parameter values used in the model appears in Table 1; in particular, we have assembled a set of parameter estimates based on composite data deriving from various EC types. Parameters not directly correlated with biological quantities have been instead

Table 1. **A summary of the parameter values used in the model**

Parameter	Value	Units	Reference
J_{Σ_1,Σ_2}	−20	NA	Scianna and Preziosi (2012)
$\boldsymbol{k}$	1	μM^{-1}	Scianna and Preziosi (2012)
J_0	4.5	NA	Calculated in this study
λ_0	4.5	NA	Scianna et al. (2011)
Ψ	1	μM^1	Calculated in this study
D_R	1	$\mu M^2 s^{-1}$	Marée et al. (2006)
k_{off_R}	1.5	s^{-1}	Marée et al. (2006)
k_{on_R}	2	s^{-1}	Marée et al. (2006)
k_{on_T}	1	$\mu M^{-1}s^{-1}$	Calculated in this study
$k_{on_{T_e}}$	2	$\mu M^{-1}s^{-1}$	Calculated in this study
T_{er}	0.2	μM	Calculated in this study
R_{n17}	3[a]	μM	Calculated in this study
T_{ex}	1[a]	μM	Calculated in this study
T_{pm}	0.2[a]	μM	Calculated in this study
k_{off_m}	2.5	s^{-1}	Calculated in this study
k_{on_m}	3.5	s^{-1}	Calculated in this study
$D_{R_{am}}$	0.1	$\mu M^2 s^{-1}$	Marée et al. (2006)
$R_{a,0}$	2	μM	Calculated in this study
$R_{i,0}$	2.5	μM	Calculated in this study

NA, not applicable.
[a]Parameters that vary in the different sets of simulations.

estimated by preliminary simulations. The behavior of the model is however fairly robust in large regions of the space around our estimates, leading to confidence in the qualitative biological relevance of the results. Initially, the cell is a round cluster with a 35 μm diameter, with defined and homogeneous levels of active and inactive Rap1 (i.e., $R_{a,0}$,$R_{i,0}$, respectively). On the contrary, the initial intracellular amount of active integrin complexes is null.

The control condition of the theoretical model is $T_{pm} = T_{ex} = R_{17} = 0$, $T_{er} = 0.2$ μM (so that $T = 0.2$ μM and no icilin stimulation.

To predict the role played in sequestering inactive Rap1 by TRPM8 channels localized in the membrane, which have indeed a cytosolic tail, we add in Eq. 2 the term $-k_{on_T} T_{pm} R_i$ ($-k_{on_{T_e}} T_{pm} R_i$ in the case of ICILIN stimulation), where T_{pm} is the concentration of membrane-bound M8. This sink term holds only for the cytololic sites in contact with the PM (i.e., $\sigma(x) = 1$ and $\exists x' \in \Omega'_x : \sigma(x') = 2$.

Finally, to reproduce different amounts (and therefore different ratios) of TRPM8 localized in either the PM or ER, we vary T_{pm} and $T_{.}$ as indicated in the corresponding plots. In particular, the amount of ER TRPM8 is changed by keeping constant the level of endogenous channels (i.e., T_{er} = 0.2 μM) while modulating the amount of exogenous TRPM8.

Online supplemental material

Supplementary figures show controls on siRNA experiments (Fig. S1) as well as supporting figures for the experiments presented in Fig. 2. Fig. S2 C shows the quantification of GFP-RBD PM recruitment. Similarly, Videos 1 and 2 show representative cells recordings in of ECs expressing GFP-RBD_{RalGDS} probe in control or cells silenced for TRPM8. Representations of model cells as well as mathematical simulations experiments are shown in Fig. S3. Fig. S4 (A and B) shows Ca^{2+} imaging and electrophysiology experiments to prove TRPM8 channel function. Figs. S4 (C–E) and S5 show adhesion experiments expressed as nonnormalized values. Controls for PLA experiments shown in Fig. 5 are reported in Fig. S5 G. Fig. S6 shows complete immunoprecipitation and GST pull-down results in support of Fig. 5.

Acknowledgments

We thank Mr. Allart, Mrs. Kakanou Ngassie, and Mrs. Zicola for technical assistance. We thank Dr. Bidaux for providing $TRPM8^{Y905A}$ pore mutant plasmids and Professor Bussolati for providing BTECs and HMECs.

This study was supported by the Ministère de l'Education Nationale and the Institut National de la Sante et de la Recherche Medicale. M. Bernardini, A. Fiorio Pla, N. Prevarskaya, and D. Gkika were supported by the Institut National du Cancer (grant INCa-PLB IO14-213). D. Gkika was supported by the Fondation ARC pour la recherche sur le cancer (grant PJA 20141202010) and the Association pour la Recherche sur les Tumeurs de la Prostate. A. Fiorio Pla was supported by grants from the University of Torino and Compagnia di San Paolo (grant Torino_call2014_L2_130). G. Serini was supported by the Associazione Italiana per la Ricerca sul Cancro (grant IG #9211 and #16702) and the Associazione Augusto per la Vita and Fondazione Piemontese per la Ricerca sul Cancro (grant ONLUS, MIUR 2010 VASCHETTO - 5 per mille 2010 MIUR). M. Bernardini was supported by the 2012-Université Franco Italienne "Vinci" program.

The authors declare no competing financial interests.

Submitted: 4 June 2015
Revised: 26 June 2016
Accepted: 12 April 2017

References

Baez, D., N. Raddatz, G. Ferreira, C. Gonzalez, and R. Latorre. 2014. Gating of thermally activated channels. *Curr. Top. Membr.* 74:51–87. http://dx.doi.org/10.1016/B978-0-12-800181-3.00003-8

Bavencoffe, A., D. Gkika, A. Kondratskyi, B. Beck, A.-S. Borowiec, G. Bidaux, J. Busserolles, A. Eschalier, Y. Shuba, R. Skryma, and N. Prevarskaya. 2010. The transient receptor potential channel TRPM8 is inhibited via the α 2A adrenoreceptor signaling pathway. *J. Biol. Chem.* 285:9410–9419. http://dx.doi.org/10.1074/jbc.M109.069377

Bazzoni, G., D.T. Shih, C.A. Buck, and M.E. Hemler. 1995. Monoclonal antibody 9EG7 defines a novel β 1 integrin epitope induced by soluble ligand and

manganese, but inhibited by calcium. *J. Biol. Chem.* 270:25570–25577. http://dx.doi.org/10.1074/jbc.270.43.25570

Bidaux, G., M. Flourakis, S. Thebault, A. Zholos, B. Beck, D. Gkika, M. Roudbaraki, J.-L. Bonnal, B. Mauroy, Y. Shuba, et al. 2007. Prostate cell differentiation status determines transient receptor potential melastatin member 8 channel subcellular localization and function. *J. Clin. Invest.* 117:1647–1657. http://dx.doi.org/10.1172/JCI30168

Bidaux, G., M. Sgobba, L. Lemonnier, A.-S. Borowiec, L. Noyer, S. Jovanovic, A.V. Zholos, and S. Haider. 2015. Functional and modeling studies of the transmembrane region of the TRPM8 channel. *Biophys. J.* 109:1840–1851. http://dx.doi.org/10.1016/j.bpj.2015.09.027

Bivona, T.G., and M.R. Philips. 2005. Analysis of Ras and Rap activation in living cells using fluorescent Ras binding domains. *Methods.* 37:138–145. http://dx.doi.org/10.1016/j.ymeth.2005.05.022

Bivona, T.G., H.H. Wiener, I.M. Ahearn, J. Silletti, V.K. Chiu, and M.R. Philips. 2004. Rap1 up-regulation and activation on plasma membrane regulates T cell adhesion. *J. Cell Biol.* 164:461–470. http://dx.doi.org/10.1083/jcb.200311093

Boettner, B., and L. Van Aelst. 2009. Control of cell adhesion dynamics by Rap1 signaling. *Curr. Opin. Cell Biol.* 21:684–693. http://dx.doi.org/10.1016/j.ceb.2009.06.004

Bos, J.L. 2005. Linking Rap to cell adhesion. *Curr. Opin. Cell Biol.* 17:123–128. http://dx.doi.org/10.1016/j.ceb.2005.02.009

Bourne, H.R., D.A. Sanders, and F. McCormick. 1990. The GTPase superfamily: A conserved switch for diverse cell functions. *Nature.* 348:125–132. http://dx.doi.org/10.1038/348125a0

Burgess, A., S. Vigneron, E. Brioudes, J.-C. Labbé, T. Lorca, and A. Castro. 2010. Loss of human Greatwall results in G2 arrest and multiple mitotic defects due to deregulation of the cyclin B-Cdc2/PP2A balance. *Proc. Natl. Acad. Sci. USA.* 107:12564–12569. http://dx.doi.org/10.1073/pnas.0914191107

Bussolati, B., I. Deambrosis, S. Russo, M.C. Deregibus, and G. Camussi. 2003. Altered angiogenesis and survival in human tumor-derived endothelial cells. *FASEB J.* 17:1159–1161.

Bussolino, F., F. Caccavari, D. Valdembri, and G. Serini. 2009. Angiogenesis: A balancing act between integrin activation and inhibition? *Eur. Cytokine Netw.* 20:191–196.

Cao, E., M. Liao, Y. Cheng, and D. Julius. 2013. TRPV1 structures in distinct conformations reveal activation mechanisms. *Nature.* 504:113–118. http://dx.doi.org/10.1038/nature12823

Carmona, G., S. Göttig, A. Orlandi, J. Scheele, T. Bäuerle, M. Jugold, F. Kiessling, R. Henschler, A.M. Zeiher, S. Dimmeler, and E. Chavakis. 2009. Role of the small GTPase Rap1 for integrin activity regulation in endothelial cells and angiogenesis. *Blood.* 113:488–497. http://dx.doi.org/10.1182/blood-2008-02-138438

Cassoni, P., T. Marrocco, B. Bussolati, E. Allia, L. Munaron, A. Sapino, and G. Bussolati. 2006. Oxytocin induces proliferation and migration in immortalized human dermal microvascular endothelial cells and human breast tumor-derived endothelial cells. *Mol. Cancer Res.* 4:351–359. http://dx.doi.org/10.1158/1541-7786.MCR-06-0024

Chadha, K.C., B. Nair, A. Godoy, R. Rajnarayanan, E. Nabi, R. Zhou, N.R. Patel, R. Aalinkeel, S.A. Schwartz, and G.J. Smith. 2015. Anti-angiogenic activity of PSA-derived peptides. *Prostate.* 75:1285–1299. http://dx.doi.org/10.1002/pros.23010

Chrzanowska-Wodnicka, M., A.E. Kraus, D. Gale, G.C. White II, and J. Vansluys. 2008. Defective angiogenesis, endothelial migration, proliferation, and MAPK signaling in Rap1b-deficient mice. *Blood.* 111:2647–2656. http://dx.doi.org/10.1182/blood-2007-08-109710

Ding, X., Z. He, Y. Shi, Q. Wang, and Y. Wang. 2010. Targeting TRPC6 channels in oesophageal carcinoma growth. *Expert Opin. Ther. Targets.* 14:513–527. http://dx.doi.org/10.1517/14728221003733602

Fink, C.C., B. Slepchenko, I.I. Moraru, J. Watras, J.C. Schaff, and L.M. Loew. 2000. An image-based model of calcium waves in differentiated neuroblastoma cells. *Biophys. J.* 79:163–183. http://dx.doi.org/10.1016/S0006-3495(00)76281-3

Fiorio Pla, A., and D. Gkika. 2013. Emerging role of TRP channels in cell migration: From tumor vascularization to metastasis. *Front. Physiol.* 4:311. http://dx.doi.org/10.3389/fphys.2013.00311

Fiorio Pla, A., and L. Munaron. 2014. Functional properties of ion channels and transporters in tumour vascularization. *Philos. Trans. R. Soc. Lond. B Biol. Sci.* 369:20130103. http://dx.doi.org/10.1098/rstb.2013.0103

Fiorio Pla, A., C. Grange, S. Antoniotti, C. Tomatis, A. Merlino, B. Bussolati, and L. Munaron. 2008. Arachidonic acid-induced Ca2+ entry is involved in early steps of tumor angiogenesis. *Mol. Cancer Res.* 6:535–545. http://dx.doi.org/10.1158/1541-7786.MCR-07-0271

Fiorio Pla, A., T. Genova, E. Pupo, C. Tomatis, A. Genazzani, R. Zaninetti, and L. Munaron. 2010. Multiple roles of protein kinase a in arachidonic acid-mediated Ca2+ entry and tumor-derived human endothelial cell migration. *Mol. Cancer Res.* 8:1466–1476. http://dx.doi.org/10.1158/1541-7786.MCR-10-0002

Fiorio Pla, A., D. Avanzato, L. Munaron, and I.S. Ambudkar. 2012a. Ion channels and transporters in cancer. 6. Vascularizing the tumor: TRP channels as molecular targets. *Am. J. Physiol. Cell Physiol.* 302:C9–C15. http://dx.doi.org/10.1152/ajpcell.00280.2011

Fiorio Pla, A., H.L. Ong, K.T. Cheng, A. Brossa, B. Bussolati, T. Lockwich, B. Paria, L. Munaron, and I.S. Ambudkar. 2012b. TRPV4 mediates tumor-derived endothelial cell migration via arachidonic acid-activated actin remodeling. *Oncogene.* 31:200–212. http://dx.doi.org/10.1038/onc.2011.231

Fonsato, V., S. Buttiglieri, M.C. Deregibus, B. Bussolati, E. Caselli, D. Di Luca, and G. Camussi. 2008. PAX2 expression by HHV-8-infected endothelial cells induced a proangiogenic and proinvasive phenotype. *Blood.* 111:2806–2815. http://dx.doi.org/10.1182/blood-2007-04-085555

Fortier, A.H., J.W. Holaday, H. Liang, C. Dey, D.K. Grella, J. Holland-Linn, H. Vu, S.M. Plum, and B.J. Nelson. 2003. Recombinant prostate specific antigen inhibits angiogenesis in vitro and in vivo. *Prostate.* 56:212–219. http://dx.doi.org/10.1002/pros.10256

Francavilla, C., L. Maddaluno, and U. Cavallaro. 2009. The functional role of cell adhesion molecules in tumor angiogenesis. *Semin. Cancer Biol.* 19:298–309. http://dx.doi.org/10.1016/j.semcancer.2009.05.004

Gkika, D., and N. Prevarskaya. 2009. Molecular mechanisms of TRP regulation in tumor growth and metastasis. *Biochim. Biophys. Acta.* 1793:953–958. http://dx.doi.org/10.1016/j.bbamcr.2008.11.010

Gkika, D., and N. Prevarskaya. 2011. TRP channels in prostate cancer: The good, the bad and the ugly? *Asian J. Androl.* 13:673–676. http://dx.doi.org/10.1038/aja.2011.18

Gkika, D., M. Flourakis, L. Lemonnier, and N. Prevarskaya. 2010. PSA reduces prostate cancer cell motility by stimulating TRPM8 activity and plasma membrane expression. *Oncogene.* 29:4611–4616. http://dx.doi.org/10.1038/onc.2010.210

Gkika, D., L. Lemonnier, G. Shapovalov, D. Gordienko, C. Poux, M. Bernardini, A. Bokhobza, G. Bidaux, C. Degerny, K. Verreman, et al. 2015. TRP channel-associated factors are a novel protein family that regulates TRPM8 trafficking and activity. *J. Cell Biol.* 208:89–107. http://dx.doi.org/10.1083/jcb.201402076

Glazier, J.A., and F. Graner. 1993. Simulation of the differential adhesion driven rearrangement of biological cells. *Phys. Rev. E Stat. Phys. Plasmas Fluids Relat. Interdiscip. Topics.* 47:2128–2154.

Gloerich, M., and J.L. Bos. 2011. Regulating Rap small G-proteins in time and space. *Trends Cell Biol.* 21:615–623. http://dx.doi.org/10.1016/j.tcb.2011.07.001

Graner, F., and J.A. Glazier. 1992. Simulation of biological cell sorting using a two-dimensional extended Potts model. *Phys. Rev. Lett.* 69:2013–2016. http://dx.doi.org/10.1103/PhysRevLett.69.2013

Grange, C., B. Bussolati, S. Bruno, V. Fonsato, A. Sapino, and G. Camussi. 2006. Isolation and characterization of human breast tumor-derived endothelial cells. *Oncol. Rep.* 15:381–386.

Grolez, G.P., and D. Gkika. 2016. TRPM8 puts the chill on prostate cancer. *Pharmaceuticals (Basel).* 9:44. http://dx.doi.org/10.3390/ph9030044

Henshall, S.M., D.E.H. Afar, J. Hiller, L.G. Horvath, D.I. Quinn, K.K. Rasiah, K. Gish, D. Willhite, J.G. Kench, M. Gardiner-Garden, et al. 2003. Survival analysis of genome-wide gene expression profiles of prostate cancers identifies new prognostic targets of disease relapse. *Cancer Res.* 63:4196–4203.

Ising, E. 1925. Beitrag zur theorie des ferromagnetismus. Zeitschrift für Physik. 31:253–258. http://dx.doi.org/10.1007/BF02980577

Jacquemet, G., H. Baghirov, M. Georgiadou, H. Sihto, E. Peuhu, P. Cettour-Janet, T. He, M. Perälä, P. Kronqvist, H. Joensuu, and J. Ivaska. 2016. L-type calcium channels regulate filopodia stability and cancer cell invasion downstream of integrin signalling. *Nat. Commun.* 7:13297. http://dx.doi.org/10.1038/ncomms13297

Johnson, C.D., D. Melanaphy, A. Purse, S.A. Stokesberry, P. Dickson, and A.V. Zholos. 2009. Transient receptor potential melastatin 8 channel involvement in the regulation of vascular tone. *Am. J. Physiol. Heart Circ. Physiol.* 296:H1868–H1877. http://dx.doi.org/10.1152/ajpheart.01112.2008

Joly, D., S. Ishibe, C. Nickel, Z. Yu, S. Somlo, and L.G. Cantley. 2006. The polycystin 1-C-terminal fragment stimulates ERK-dependent spreading of renal epithelial cells. *J. Biol. Chem.* 281:26329–26339. http://dx.doi.org/10.1074/jbc.M601373200

Klasen, K., D. Hollatz, S. Zielke, G. Gisselmann, H. Hatt, and C.H. Wetzel. 2012. The TRPM8 ion channel comprises direct Gq protein-activating capacity. *Pflugers Arch.* 463:779–797. http://dx.doi.org/10.1007/s00424-012-1098-7

Korff, T., T. Krauss, and H.G. Augustin. 2004. Three-dimensional spheroidal culture of cytotrophoblast cells mimics the phenotype and differentiation of cytotrophoblasts from normal and preeclamptic pregnancies. *Exp. Cell Res.* 297:415–423. http://dx.doi.org/10.1016/j.yexcr.2004.03.043

Lafuente, E.M., A.A.F.L. van Puijenbroek, M. Krause, C.V. Carman, G.J. Freeman, A. Berezovskaya, E. Constantine, T.A. Springer, F.B. Gertler, and V.A. Boussiotis. 2004. RIAM, an Ena/VASP and Profilin ligand, interacts with Rap1-GTP and mediates Rap1-induced adhesion. *Dev. Cell.* 7:585–595. http://dx.doi.org/10.1016/j.devcel.2004.07.021

Lenter, M., H. Uhlig, A. Hamann, P. Jenö, B. Imhof, and D. Vestweber. 1993. A monoclonal antibody against an activation epitope on mouse integrin chain β 1 blocks adhesion of lymphocytes to the endothelial integrin α 6 β 1. *Proc. Natl. Acad. Sci. USA.* 90:9051–9055. http://dx.doi.org/10.1073/pnas.90.19.9051

Liao, M., E. Cao, D. Julius, and Y. Cheng. 2013. Structure of the TRPV1 ion channel determined by electron cryo-microscopy. *Nature.* 504:107–112. http://dx.doi.org/10.1038/nature12822

Lilja, J., T. Zacharchenko, M. Georgiadou, G. Jacquemet, N. Franceschi, E. Peuhu, H. Hamidi, J. Pouwels, V. Martens, F.H. Nia, et al. 2017. SHANK proteins limit integrin activation by directly interacting with Rap1 and R-Ras. *Nat. Cell Biol.* 19:292–305. http://dx.doi.org/10.1038/ncb3487

Marée, A.F.M., A. Jilkine, A. Dawes, V.A. Grieneisen, and L. Edelstein-Keshet. 2006. Polarization and movement of keratocytes: A multiscale modelling approach. *Bull. Math. Biol.* 68:1169–1211. http://dx.doi.org/10.1007/s11538-006-9131-7

Mergler, S., C. Mertens, M. Valtink, P.S. Reinach, V.C. Székely, N. Slavi, F. Garreis, S. Abdelmessih, E. Türker, G. Fels, and U. Pleyer. 2013. Functional significance of thermosensitive transient receptor potential melastatin channel 8 (TRPM8) expression in immortalized human corneal endothelial cells. *Exp. Eye Res.* 116:337–349. http://dx.doi.org/10.1016/j.exer.2013.10.003

Metropolis, N. 1953. Equation of state calculations by fast computing machines. *J. Chem. Phys.* 21:1087–1092. http://dx.doi.org/10.1063/1.1699114

Nilius, B. 2007. TRP channels in disease. *Biochim. Biophys. Acta.* 1772:805–812. http://dx.doi.org/10.1016/j.bbadis.2007.02.002

Pillozzi, S., M.F. Brizzi, P.A. Bernabei, B. Bartolozzi, R. Caporale, V. Basile, V. Boddi, L. Pegoraro, A. Becchetti, and A. Arcangeli. 2007. VEGFR-1 (FLT-1), β1 integrin, and hERG K+ channel for a macromolecular signaling complex in acute myeloid leukemia: Role in cell migration and clinical outcome. *Blood.* 110:1238–1250. http://dx.doi.org/10.1182/blood-2006-02-003772

Potente, M., H. Gerhardt, and P. Carmeliet. 2011. Basic and therapeutic aspects of angiogenesis. *Cell.* 146:873–887. http://dx.doi.org/10.1016/j.cell.2011.08.039

Potts, R. 1952. Some generalized order-disorder transformations. *Math. Proc. Cambridge.* 48:106–109. http://dx.doi.org/10.1017/S0305004100027419

Prevarskaya, N., R. Skryma, and Y. Shuba. 2010. Ion channels and the hallmarks of cancer. *Trends Mol. Med.* 16:107–121. http://dx.doi.org/10.1016/j.molmed.2010.01.005

Pupo, E., A.F. Pla, D. Avanzato, F. Moccia, J.-E.A. Cruz, F. Tanzi, A. Merlino, D. Mancardi, and L. Munaron. 2011. Hydrogen sulfide promotes calcium signals and migration in tumor-derived endothelial cells. *Free Radic. Biol. Med.* 51:1765–1773. http://dx.doi.org/10.1016/j.freeradbiomed.2011.08.007

Reedquist, K.A., E. Ross, E.A. Koop, R.M. Wolthuis, F.J. Zwartkruis, Y. van Kooyk, M. Salmon, C.D. Buckley, and J.L. Bos. 2000. The small GTPase, Rap1, mediates CD31-induced integrin adhesion. *J. Cell Biol.* 148:1151–1158. http://dx.doi.org/10.1083/jcb.148.6.1151

Riou, P., S. Kjær, R. Garg, A. Purkiss, R. George, R.J. Cain, G. Bineva, N. Reymond, B. McColl, A.J. Thompson, et al. 2013. 14-3-3 proteins interact with a hybrid prenyl-phosphorylation motif to inhibit G proteins. *Cell.* 153:640–653. (published erratum appears in *Cell.* 2013. 153:1164.) http://dx.doi.org/10.1016/j.cell.2013.03.044

Sandri, C., F. Caccavari, D. Valdembri, C. Camillo, S. Veltel, M. Santambrogio, L. Lanzetti, F. Bussolino, J. Ivaska, and G. Serini. 2012. The R-Ras/RIN2/Rab5 complex controls endothelial cell adhesion and morphogenesis via active integrin endocytosis and Rac signaling. *Cell Res.* 22:1479–1501. http://dx.doi.org/10.1038/cr.2012.110

Schwab, A., A. Fabian, P.J. Hanley, and C. Stock. 2012. Role of ion channels and transporters in cell migration. *Physiol. Rev.* 92:1865–1913. http://dx.doi.org/10.1152/physrev.00018.2011

Scianna, M., and L. Preziosi. 2012. Multiscale developments of the cellular Potts model. *Multiscale Model. Simul.* 10:342–382. http://dx.doi.org/10.1137/100812951

Scianna, M., and L. Preziosi. 2013. Modeling the influence of nucleus elasticity on cell invasion in fiber networks and microchannels. *J. Theor. Biol.* 317:394–406. http://dx.doi.org/10.1016/j.jtbi.2012.11.003

Scianna, M., L. Munaron, and L. Preziosi. 2011. A multiscale hybrid approach for vasculogenesis and related potential blocking therapies. *Prog. Biophys. Mol. Biol.* 106:450–462. http://dx.doi.org/10.1016/j.pbiomolbio.2011.01.004

Scianna, M., L. Preziosi, and K. Wolf. 2013. A cellular Potts model simulating cell migration on and in matrix environments. *Math. Biosci. Eng.* 10:235–261. http://dx.doi.org/10.3934/mbe.2013.10.235

Serini, G., D. Valdembri, S. Zanivan, G. Morterra, C. Burkhardt, F. Caccavari, L. Zammataro, L. Primo, L. Tamagnone, M. Logan, et al. 2003. Class 3 semaphorins control vascular morphogenesis by inhibiting integrin function. *Nature.* 424:391–397. http://dx.doi.org/10.1038/nature01784

Serini, G., D. Valdembri, and F. Bussolino. 2006. Integrins and angiogenesis: A sticky business. *Exp. Cell Res.* 312:651–658. http://dx.doi.org/10.1016/j.yexcr.2005.10.020

Steinberg, M.S. 1970. Does differential adhesion govern self-assembly processes in histogenesis? Equilibrium configurations and the emergence of a hierarchy among populations of embryonic cells. *J. Exp. Zool.* 173:395–433. http://dx.doi.org/10.1002/jez.1401730406

Sun, J., T. Yang, P. Wang, S. Ma, Z. Zhu, Y. Pu, L. Li, Y. Zhao, S. Xiong, D. Liu, and Z. Zhu. 2014. Activation of cold-sensing transient receptor potential melastatin subtype 8 antagonizes vasoconstriction and hypertension through attenuating RhoA/Rho kinase pathway. *Hypertension.* 63:1354–1363. http://dx.doi.org/10.1161/HYPERTENSIONAHA.113.02573

Thebault, S., L. Lemonnier, G. Bidaux, M. Flourakis, A. Bavencoffe, D. Gordienko, M. Roudbaraki, P. Delcourt, Y. Panchin, Y. Shuba, et al. 2005a. Novel role of cold/menthol-sensitive transient receptor potential melastatine family member 8 (TRPM8) in the activation of store-operated channels in LNCaP human prostate cancer epithelial cells. *J. Biol. Chem.* 280:39423–39435. http://dx.doi.org/10.1074/jbc.M503544200

Thebault, S., A. Zholos, A. Enfissi, C. Slomianny, E. Dewailly, M. Roudbaraki, J. Parys, and N. Prevarskaya. 2005b. Receptor-operated Ca2+ entry mediated by TRPC3/TRPC6 proteins in rat prostate smooth muscle (PS1) cell line. *J. Cell. Physiol.* 204:320–328. http://dx.doi.org/10.1002/jcp.20301

Thebault, S., M. Flourakis, K. Vanoverberghe, F. Vandermoere, M. Roudbaraki, V. Lehen'kyi, C. Slomianny, B. Beck, P. Mariot, J.-L. Bonnal, et al. 2006. Differential role of transient receptor potential channels in Ca2+ entry and proliferation of prostate cancer epithelial cells. *Cancer Res.* 66:2038–2047. http://dx.doi.org/10.1158/0008-5472.CAN-05-0376

Thodeti, C.K., B. Matthews, A. Ravi, A. Mammoto, K. Ghosh, A.L. Bracha, and D.E. Ingber. 2009. TRPV4 channels mediate cyclic strain-induced endothelial cell reorientation through integrin-to-integrin signaling. *Circ. Res.* 104:1123–1130. http://dx.doi.org/10.1161/CIRCRESAHA.108.192930

Tsai, F.-C., A. Seki, H.W. Yang, A. Hayer, S. Carrasco, S. Malmersjö, and T. Meyer. 2014. A polarized Ca2+, diacylglycerol and STIM1 signalling system regulates directed cell migration. *Nat. Cell Biol.* 16:133–144. http://dx.doi.org/10.1038/ncb2906

Tsavaler, L., M.H. Shapero, S. Morkowski, and R. Laus. 2001. Trp-p8, a novel prostate-specific gene, is up-regulated in prostate cancer and other malignancies and shares high homology with transient receptor potential calcium channel proteins. *Cancer Res.* 61:3760–3769.

van den Berghe, N., R.H. Cool, G. Horn, and A. Wittinghofer. 1997. Biochemical characterization of C3G: An exchange factor that discriminates between Rap1 and Rap2 and is not inhibited by Rap1A(S17N). *Oncogene.* 15:845–850. http://dx.doi.org/10.1038/sj.onc.1201407

van der Flier, A., K. Badu-Nkansah, C.A. Whittaker, D. Crowley, R.T. Bronson, A. Lacy-Hulbert, and R.O. Hynes. 2010. Endothelial α5 and αv integrins cooperate in remodeling of the vasculature during development. *Development.* 137:2439–2449. http://dx.doi.org/10.1242/dev.049551

Vrenken, K.S., K. Jalink, F.N. van Leeuwen, and J. Middelbeek. 2015. Beyond ion-conduction: Channel-dependent and -independent roles of TRP channels during development and tissue homeostasis. *Biochim. Biophys. Acta.* 1863:1436–1446.

Wang, Y., H. He, N. Srivastava, S. Vikarunnessa, Y.B. Chen, J. Jiang, C.W. Cowan, and X. Zhang. 2012. Plexins are GTPase-activating proteins for Rap and are activated by induced dimerization. *Sci. Signal.* 5:ra6. http://dx.doi.org/10.1126/scisignal.2002636

Wondergem, R., T.W. Ecay, F. Mahieu, G. Owsianik, and B. Nilius. 2008. HGF/SF and menthol increase human glioblastoma cell calcium and migration.

Biochem. Biophys. Res. Commun. 372:210–215. http://dx.doi.org/10.1016/j.bbrc.2008.05.032

Yee, N.S., W. Zhou, and M. Lee. 2010. Transient receptor potential channel TRPM8 is over-expressed and required for cellular proliferation in pancreatic adenocarcinoma. *Cancer Lett.* 297:49–55. http://dx.doi.org/10.1016/j.canlet.2010.04.023

Zhang, L., and G.J. Barritt. 2006. TRPM8 in prostate cancer cells: A potential diagnostic and prognostic marker with a secretory function? *Endocr. Relat. Cancer.* 13:27–38. http://dx.doi.org/10.1677/erc.1.01093

Zhang, X., S. Mak, L. Li, A. Parra, B. Denlinger, C. Belmonte, and P.A. McNaughton. 2012. Direct inhibition of the cold-activated TRPM8 ion channel by Gαq. *Nat. Cell Biol.* 14:851–858. http://dx.doi.org/10.1038/ncb2529